Alma Mater Studiorum - Università di Bologna

DOTTORATO DI RICERCA IN

MONITORAGGIO E GESTIONE DELLE STRUTTURE E DELL'AMBIENTE - SEHM2

Ciclo 34

Settore Concorsuale: 08/B2 - SCIENZA DELLE COSTRUZIONI

Settore Scientifico Disciplinare: ICAR/08 - SCIENZA DELLE COSTRUZIONI

STRUCTURAL HEALTH MONITORING OF STORAGE TANKS

Presentata da: Denis Bogomolov

Coordinatore Dottorato

Alessandro Marzani

Supervisore

Alessandro Marzani

Co-supervisore

Luca De Marchi

Co-supervisore

Nicola Testoni

Esame finale anno 2022

Ph.D. thesis titled " Structural Health Monitoring of Storage Tanks ".

Ph.D candidate – Denis Bogomolov

Abstract

In oil depots and fuel storage facilities, undetected storage tanks damages can lead to the leakage of the oil stored in the soil leading to pollution and economical losses. Leaks are generally due to the perforation of the storage tank floor or wall because of corrosion. The detection of corrosion and leaks is a complicated task, especially for operative tanks with inaccessible floor for detailed inspections and is generally attempted by mean of acoustic emission systems operating from the outer skin of the tank.

In this thesis, Ph.D candidate presents a compact sensor node (SN) designed for long-term and real-time acoustic emission monitoring of above ground storage tanks (ASTs). Each SN exploits up to three inexpensive low-frequency sensors based on piezoelectric diaphragms for effective leakage detection, and it is capable by means of built-in Digital Signal Processing functionalities to process the acquired time waveforms extracting the AE features usually required by testing protocols. Alternatively, capability to plug three high frequency AE sensors to a SN for corrosion simulated phenomena detection is envisaged and demonstrated.

Another innovative aspect that the Ph.D candidate presents in this work is an alternative mathematical model of corrosion location on the bottom of the AST. This approach implies considering the three-dimensional localization model versus the two-dimensional commonly used according to the literature. This approach is aimed at significant optimization in the number of sensors in relation to the standard approach for solving localization problems as well as to allow filtering the false AE events related to the condensate droplets from AST ceiling. The technological implementation of this concept required the solution of a number of technical problems, such as the precise time of arrival (ToA) signal estimation, vertical localization of the AE source and multilaration solution that were discussed in detail in this work.

To validate the developed prototype, several experimental campaigns were organized that included the simulation of target phenomena both in laboratory conditions and on a real water storage tank. At the first testing stage, the developed prototype was subjected to laboratory tests for sensitivity and the relatively long monitoring mode verification. Next focus of the study was shifted to a small water tank to investigate waves propagation related to simulated AE corrosion and to validate the sensitivity of SN to bulk waves expected in ASTs. Finally, an experimental validation on a floating-roof AST 17 m high and 18 m in diameter, filled with water to a level of about 6.2 m, is proposed for both leak and corrosion simulations. Leaks were induced by opening and closing a drainage valve existing at the bottom skirt of the storage tank while acoustic emission signals were recorded at three sensors and processed in real time. In particular, designed nozzles of different diameter, from 1 mm to 9 mm, where used to simulate leakages of different entities. The testing results confirmed the possibility of detecting and monitoring leaks of various diameters in the low-frequency region (1 - 2 kHz) not traditionally considered by state-of-art acoustic-emission monitoring systems. Then, to simulate the source of bottom corrosion, a unique experimental setup was designed to place an electrically insulated piezo emitter inside the tank. Preliminary results confirm the high accuracy of the proposed concept and the mathematical model of three-dimensional corrosion localization in AST bottoms.

Declaration of an oath

I hereby declare in lieu of an oath that I have written this thesis independently and without the use of other than the stated in the text aids. All passages taken verbatim or in spirit from published and unpublished writings are marked as such. The work has not yet been submitted in the same or similar form or in excerpts within the framework of another examination.

Denis Bogomolov

Bologna, Italy, 15.05.2022

Contents

List of Figures

List of Tables

Acknowledgements

The Ph.D. candidate warmly thanks his supervisor and co–advisors, namely Alessandro Marzani, Luca De Marchi and Nicola Testoni for their multidisciplinary support throughout the entire research.

Abstract

In oil depots and fuel storage facilities, undetected storage tanks damages can lead to the leakage of the oil stored in the soil leading to pollution and economical losses. Leaks are generally due to the perforation of the storage tank floor or wall because of corrosion. The detection of corrosion and leaks is a complicated task, especially for operative tanks with inaccessible floor for detailed inspections and is generally attempted by mean of acoustic emission systems operating from the outer skin of the tank.

In this thesis, Ph.D candidate presents a compact sensor node (SN) designed for long-term and real-time acoustic emission monitoring of above ground storage tanks (ASTs). Each SN exploits up to three inexpensive low-frequency sensors based on piezoelectric diaphragms for effective leakage detection, and it is capable by means of built-in Digital Signal Processing functionalities to process the acquired time waveforms extracting the AE features usually required by testing protocols. Alternatively, capability to plug three high frequency AE sensors to a SN for corrosion simulated phenomena detection is envisaged and demonstrated.

Another innovative aspect that the Ph.D candidate presents in this work is an alternative mathematical model of corrosion location on the bottom of the AST. This approach implies considering the three-dimensional localization model versus the two-dimensional commonly used according to the literature. This approach is aimed at significant optimization in the number of sensors in relation to the standard approach for solving localization problems as well as to allow filtering the false AE events related to the condensate droplets from AST ceiling. The technological implementation of this concept required the solution of a number of technical problems, such as the precise time of arrival (ToA) signal estimation, vertical localization of the AE source and multilateration solution that have been discussed in detail in this work.

To validate the developed prototype, several experimental campaigns were organized that included the simulation of target phenomena both in laboratory conditions and on a real water storage tank. At the first testing stage, the developed prototype was subjected to laboratory tests for sensitivity and the relatively long monitoring mode verification. Next focus of the study was shifted to a small water tank in order to investigate waves propagation related to simulated AE corrosion and to validate the sensitivity of SN to bulk acoustic waves expected in ASTs. Finally, an experimental validation on a floating-roof AST 17 m high and 18 m in diameter, filled with water to a level of about 6.2 m, is proposed for both leak and corrosion simulations. Leaks were induced by opening and closing a drainage valve existing at the bottom skirt of the storage tank while acoustic

emission signals were recorded at three sensors and processed in real time. In particular, designed nozzles of different diameter, from 1 mm to 9 mm, where used to simulate leakages of different entities. The testing results confirmed the possibility of detecting and monitoring leaks of various diameters in the low-frequency region ($1-2$ kHz) not traditionally considered by state-of-art acoustic-emission monitoring systems. Then, to simulate the source of bottom corrosion, a unique experimental setup was designed to place an electrically insulated piezo–emitter inside the tank. Preliminary results confirm the high accuracy of the proposed concept and the mathematical model of three-dimensional corrosion localization in AST bottoms.

1 Introduction

Aboveground Storage Tanks (AST) are widely used in various spheres of human life including the chemical, petrochemical, oil refining industries, as well as many civilian industrial facilities. In these scenarios, the presence of aggressive fluids, such as hydrocarbons or even water, often causes wear on the metal walls of such structures. In particular, metal degradation processes generally due to the interaction with corrosive environments or/and hydrogen can lead to structural failure and, as a result, downtime in production.

To obtain information about the possible degradation of the tank, various non-destructive testing (NDT) methods of inspection have been proposed including Visual Testing, Ultrasonic Testing, Potential Drop (PD) techniques, Acoustic Emission, Radiographic testing, Eddy Current Techniques and Magnetic inspection. The most of considered NDT methods are characterized by a high frequency of inspection and by the need for interruption of AST operations every 3 to 7 years, as presented in the work of Aljarah et al. (2021). However, the cost of preparing a tank for an internal inspection can easily reach 100,000 euros Lackner and Tscheliesnig (2007), so significant savings can be made through alternative approaches, such as for example, AST continuous monitoring.

In this framework, Martin (2012) found that acoustic emission is acknowledged as one of the most suitable method for long-term monitoring of storage tanks . This approach involves equipping the tank with an AE system to monitor the condition without having to shut down operations. Acoustic emission (AE) is defined by the American Society for Metals (ASM) Pollock (1989) as the class of phenomena whereby transient elastic stress waves are generated by the rapid release of energy from localized sources within a material. These elastic stress waves travel through solid and can be detected by suitable receiving devices on the solid surface, for example by proper transducers, offering a mean to detect and locate the AE source. In addition, stress waves propagating in a solid material in contact with fluids can leak part of their energy into the surrounding fluid in the form of bulk waves that allow detecting the wave source form the fluid. Thus, AE is the release of energy, originated with stress. In fact, due to an applied stress or a change of stress level in the material, irreversible plastic deformations of the material (i.e. dislocations at microscopic level), micro fractures of the material (i.e. rupture of material inclusions at microscopic level) as well as contacts between material surfaces, can take place thus originating stress waves.

Existing commercial AE systems are generally characterized by bulky and cost intensive solutions, both because of the price of the AE equipment as well as due to the high number of costly transducers, resulting suitable for short

term diagnostic inspections. In this context, the development of low-cost AE sensor networks optimized for long term monitoring is a priority task. As such, this work presents an innovative low-cost and low-weight sensor node (SN) with built-in Digital Signal Processing (DSP) functionalities which can yield light and fast deployable sensor networks for AE monitoring. The developed SN follows the paradigm of near-sensor monitoring, i.e. it has the ability to process signals in the close proximity of AE sensors deployed on the inspected object. Consequently, the length of coaxial cables traditionally used in AE instrumentation is reduced and, as an immediate by-product, the sensitivity to external noise is minimized, which is a major cause of the low signal to noise ratio of on-site AE equipment.

Another innovative proposal involves the use of an alternative configuration of AE sensors placed on the AST wall. A three-dimensional bottom corrosion localization approach for ASTs versus two-dimensional traditionally used is proposed in the thesis. It is assumed that the use of several AE sensors lines (at least three) consisting of three AE transducers each can allow to indicate both the relative distance and the relative angle indicating the position of the AE source. Moreover, the proposed model also solves the problem of spurious AE events associated with condensate droplets falling from the AST ceiling frequently described in the relevant literature, such as in Lackner and Tscheliesnig (2003b). Thus, a significant optimization of the number of AE sensors required for corrosion localization is carried out in comparison with traditional models. The corresponding mathematical model is presented in this thesis.

To validate the effectiveness of the proposed SN versatile experimental campaigns to simulate sources of leakage and AST bottom corrosion were organized. The first stage of development included laboratory tests simulating AEs using a metrological verification scheme be means of high precision measurement equipment. Then a more comprehensive testing of the prototype was performed to verify its reliability in the monitoring mode. As a next step, the focus of the study was shifted to a miniature water storage tank as a more approximated setup of AST to test the sensitivity of the SN to detect waves propagating from the water, as well as to verify the proposed source location algorithm. At the final experimental stage, the verification of the proposed algorithm for bottom source location and induced leakage monitoring were organised on an AST 17 m high and 18 m in diameter, filled with water to a level of about 6.2 m, located in one of the Eni S.p.A. storage parks (Voltaggio, Italy). To verify the location algorithm proposed, a unique experimental campaign was proposed by placing an active piezo sensor (waves exciter) inside the water tank. To imitate the leakage scenario, nine nozzles with diameter from 1 mm to 9 mm, at a step of 1 mm, were specially prepared to be used in a drainage valve of the tank. AE events were

collected by the piezoelectric sensors, directly processed in the SN to extract AE features, which were sent and monitored in real time.

The thesis is organized as follows. The section 2 reveals state-of-the-art with discussing the problem statement in detail, while the section 3 is focusing on the theoretical framework of the research. Methodology section 4 is presenting the developed AE monitoring system prototype and preliminary laboratory verification, as well as an innovative three-dimensional model for the localization of AE events associated with corrosion of the AST bottom is disclosed there. In the section 5, the results of versatile experimental campaigns aimed at AST bottom corrosion and leakage phenomena simulation are drawn, while the discussions are provided in the Section 6. Finally, conclusion are given in Section 7.

2 Literature Review

2.1 Problem statement

In oil depots and fuel storage facilities, undetected storage tanks damages can lead to the leakage of the oil stored in the soil leading to pollution and economical losses. Metal degradation, which are generally due to bottom water (brine) layer, dissolved H2S, CO2, CO4, sulfate-reducing bacteria, and sludge deposits, may cause to structural failures usually occurring at the floor sheet as described in Foroulis (1981) and Lackner and Tscheliesnig (2003a). Groups of this kind of metal degradation are commonly referred to as corrosion phenomena. Permanent perforation of the tank bottom due to corrosion, in turn, cause the leakage of the storage product and soil contamination which is destructive to the local ecosystem. The detection of such damages is a complicated task, especially for operative tanks that do not allow for detailed inspection of the floor without a complete operation shutdown.

Through periodic internal inspection and ultrasonic thickness gauging, the actual corrosion rate of the tank bottom can be determined, and subsequent repairs can ensure long-term safe operation of the tank in the future. However, this approach leads to two disadvantages in reservoir management: under-inspection or over-inspection. On the one hand, there is a risk of environmental damage caused by leaking reservoirs and the high cost of cleaning up the environment. On the other hand, there is the cost of cleaning up the tanks and the temporary loss of storage volume or operational problems in the plant, which can result from a leak or a problem with the operation of the plant, which can be extremely costly. Consequently, the most current strategy for tank owners is to extend the life span of their tanks to such an extent that the minimum bottom thickness is reached before the next scheduled inspection. These management drawbacks are the main driving factors in finding solutions that will avoid scheduled inspections or significantly increase the period between them (Martinez (2013)).

In this context, real-time damage detection by means of acoustic emission monitoring systems operating from the tank's outer skin is practically the only possible way to optimize full-inspection interval management. Above all, the market demands for more affordable yet effective alternatives to the high cost existing solutions.

2.2 Corrosion phenomena in AST bottoms

According to Speight (2014), corrosion of metals is a natural phenomenon defined as the degradation of a material or its properties as a result of a reaction with its

surroundings. This is also defeined as an electrochemical reaction, i.e. a chemical reaction that results in a direct electric current. Although there are different types of corrosion, they all require the presence of four basic components for corrosion to occur: the anode, the cathode, the metal pathway and the electrolyte. The inside of the AST, and especially its bottom, are prone to uncontrolled corrosion (Groysman (2010)). The thickness of the tank bottom can be reduced by corrosion from above on the side of the stored liquid, and from below, or "on the soil side".

Crude oil represents a mixture of a large variety (thousands) of organic substances, mainly HCs (hazardous chemical substance), with some admixture of oxygen-, nitrogen-, sulphur-containing organic compounds and some inorganic species (metals etc). HCs can be straight and branched, saturated and unsaturated aliphatic, alicyclic, aromatic and polyaromatic compounds according to Yemashova et al. (2007). Refinery products are also mixtures containing straight and branched chain hydrocarbons, alkenes, naphthalenes, aromatics and other compounds (Allsopp et al. (2004)). Oil and its derivatives as a rule are not supposed to be corrosive to metals, while the main prerequisite for corrosion development is the accumulation of water at the bottom of storage tanks. Avoiding the appearance of water in the tanks is extremely difficult. The basic sludge and water (BS&W) content of crude oil at storage and transportation facilities like pipelines is usually limited to 0.5 volume % (water + sediment), Been (2011). However, water and water vapor can penetrate into crude oil and its derivatives during storage, transportation, and some other operations (Groysman (2000)). Because of the high polarity of water molecules, water droplets separate from the organic phase on steel surfaces, forming a water cushion at the bottom of tanks, and electrochemical corrosion of steel occurs.

Bottom corrosion processes can progress even more intensively due to the upper oxygen inflow into the reservoirs as stated in Yemashova et al. (2007). The solubility of oxygen in hydrocarbons is higher (60 to 70 ppm) than in water (8 ppm), so oxygen diffuses from the organic phase (hydrocarbons or fuel) into the aqueous phase according to the solubility in each phase and the concentration gradient increases up to oxygen saturation in the aqueous phase Groysman (2005). Concentration cell corrosion may occur when a surface deposit, mill scale, or crevice creates a localized area of lower oxygen concentration API (2005). The difference in oxygen concentration between the inaccessible area and the bulk electrolyte creates a concentration cell and may result in significant localized metal loss. The extent of internal corrosion is also influenced by the temperature, CO2, H2S and salts (sodium chloride, calcium chloride, and magnesium chloride), light organic acids, etc. Some of the aggressive species are typically separated from crude during production operations performed at low pressure (atmospheric up

to 1 bar gauge pressure) or in various technological processes such as desalting and rectification of crude. In the tank, remaining aggressive variables undergo extraction from organic phase into the aqueous phase and may cause a decrease in the pH and increase in the water corrosivity. Even in the absence of abiotic corrosive factors, the bacteria are known to cause severe internal corrosion problems in crude oil storage and transport (Yemashova et al. (2007)). Ability of microorganisms to grow both in a water phase and on inter-phase of water/hydrocarbon as well as the generation of products of their metabolism worsen the physical and chemical properties of oils and fuels. Activity of microorganisms promotes an increase of suspended solids content and formation of corrosive sludge at the bottom of tanks. Microbial degradation of HCs and other organic compounds increases the water content in sludge, which can exceed 10 %. Pitting corrosion has been observed underneath sludge deposits that are a mix of sand and clay particles, water, and oil products (Been (2011)). As an example, the appearance of steel samples before and after 6 months of exposure to sludge is shown in Figure 1. Both uniform and pitting corrosion were observed.

Fretting-related corrosion may also occur on the bottoms of external floating roof tanks API (2005). Repeated, frequent contact between the bottom and the end of the pipe leg when the roof is landed, removes any protective layer of rust scale that may have formed on the bottom surface. When the roof is floated again, water on the tank bottom causes corrosion at the location on the landing plate where the coating and/or any protective rust scale has been damaged. Frequent roof landings over a long period of time causes corrosion severe and localized enough to corrode a hole through the striker plate and the floor plate like a cookie cutter. Most bottom designs require "striker plates" under each roof support leg. When the floating roof is landed, the pipe legs rest on the striker plates supporting the weight of the roof. In some cases, welding can produce large differences in the microstructure of a steel bottom plate resulting in galvanic corrosion. Preferential metal dissolution can occur at the heat-affected zones (HAZ) of the base metal near the welds.

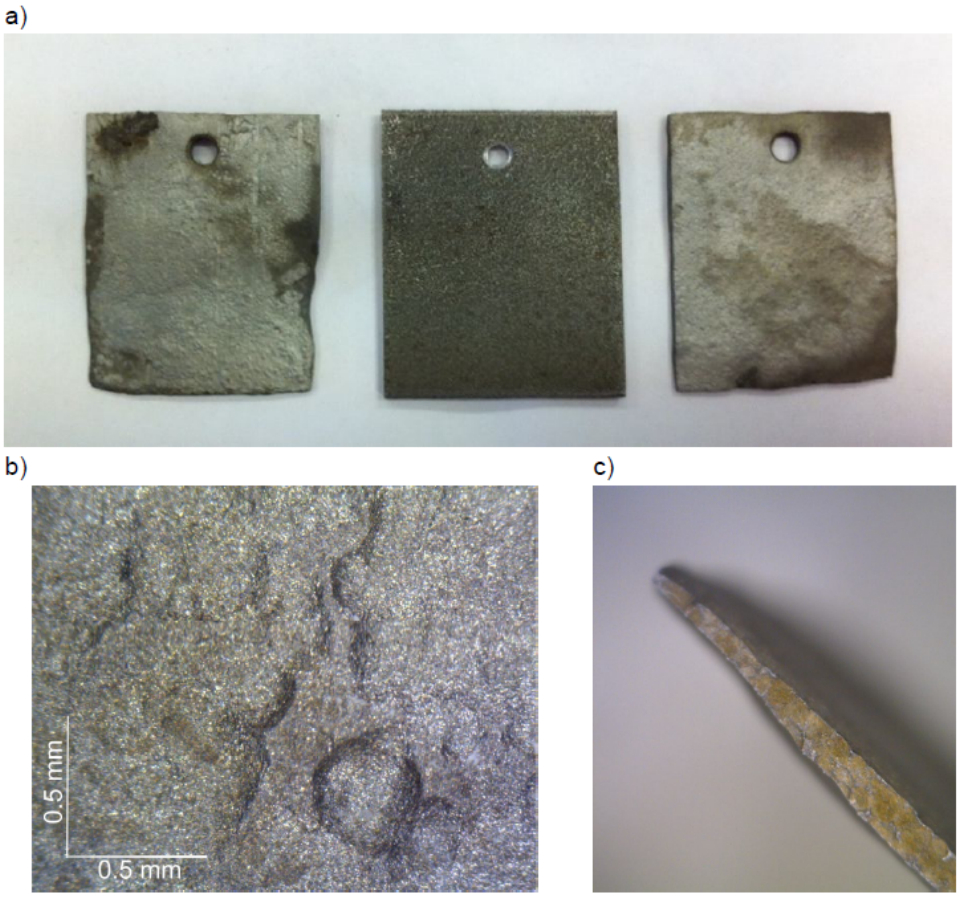

Figure 1: Corrosion of steel samples exposed to AST bottom sludge for 6 months, Martinez (2013), where a) a duplicate of the exposed specimen next to the un-exposed specimen shown in the middle, b) localized pitting corrosion attack and c) general corrosion visible trough thinning of the specimen.

2.3 Leaks in AST

One of the environmental impacts that can result from tank farm operation is an oil spill due to leaks. The area where each activity is associated with tank farm operation has the potential risk of a spill causing contamination of surrounding soil and rivers, in accord with Tadros (2020). Leakage can occur as a result of the development of corrosion processes both on the wall and on the bottom of the tank. Free internet sources (InspectAPedia) also mention improper operation (such as incomplete closure of valves) and poor repair as other common causes of leaks. A couple of examples of the appearance of a leak on the wall of a storage tank are demonstrated in Figure 2.

Figure 2: Active leaks at the AST wall due to corrosive perforations, Generis (2019).

2.4 Acoustic Emission Inspection of ASTs

The detection of corrosion and leaks is a complicated task, especially for operative tanks with inaccessible floor for detailed inspections and is generally attempted by means of acoustic emission testing, operating from the outer skin of the tank. However, standardised approaches for non-destructive testing of the tank, including AE testing (ISO and AST), involve finding defective areas as a temporary inspection carried out over a period of 3 to 7 years to keep the tank operating cost-effectively. It is also evident that metal degradation can start at any time and periodic inspection can reveal the resolution at a critical stage. Another obvious disadvantage of periodic AE inspections is that even if there are active sources of degradation, it is difficult to establish the criticality of such events because in this context the previous trend history of AE parameters is unknown. Therefore, there is a high demand for cost-effective technology to enable long-term, continuous monitoring of AST.

In the context of storage tanks long-term monitoring, the AE method is thought of as one of the most applicable and promising candidate having an advantage over other methods in many technical aspects. This is primarily due to the passive registration of active AE sources, which allows mapping large areas of the tank without a probing signal. The standard strategy for a bi-dimensional localization of AE events at the bottom of the tank, as described in Riahi and Shamekh (2006), is based on the fact that high-frequency pressure waves, generated from the bottom of the storage tank because of a structural change (source), radiate in the fluid from the source to the tank outer cylindrical wall, cross the cylindrical wall thickness reaching thus the outer surface of the cylindrical tank. To capture the related waves propagation, the approach uses an array of AE sensors, distributed around the tank along a circular ring generally positioned at a height of 0,5–3 meters. Next, the acquired signal are properly processed

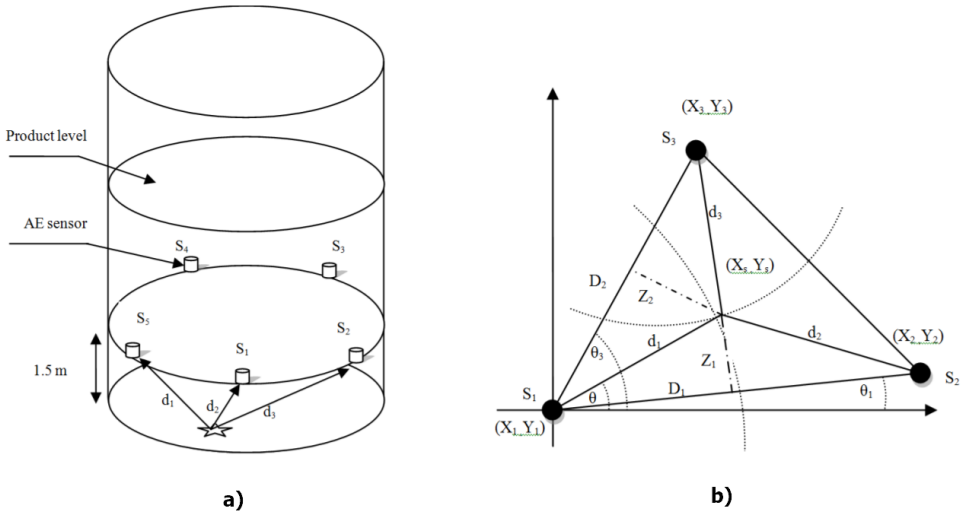

Figure 3: Standard AE inspection of AST where a) AE sensors arrangement, b) AE source location in two dimensions using triangulation method.

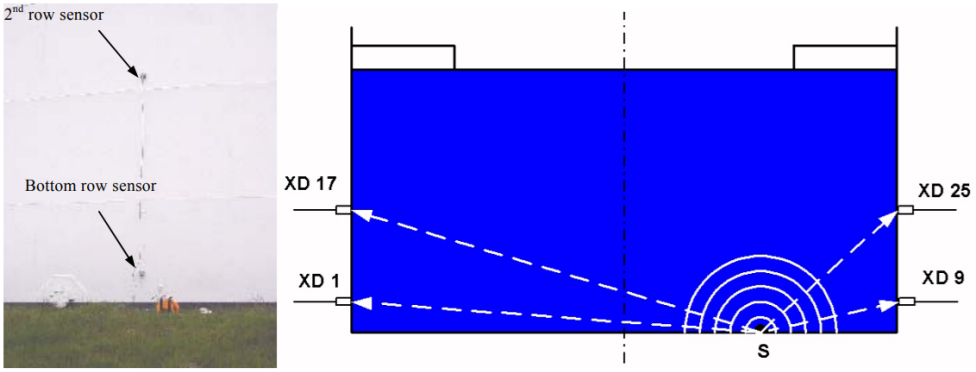

Figure 4: Double-ring arrangement of AE sensors on an AST.

to estimate the position of the AE source (CBS EN 15856:2010, NDT (2010)). Single-tier arrangement of sensors and the principle of localization of AE events are given the Figure 3 and described in detail in Hodaei et al. (2012).

Alternatively, the use of two rings around the tank allows to distinguish the acoustic emission sources arriving from the top of the tank, often associated with condensate drops falling from the ceiling, to those related to corrosion of the bottom floor, reducing thus false AE events. The second ring of AE sensors usually placed at 5-6 meters height from the ground. Double-ring arrangement of AE sensors is illustrated in the Figure 4 and with detailed description of localization stages disclosed in Lackner and Tscheliesnig (2003b). Despite the presence of two levels of sensors, the upper ring is used only for filtering out false events coming from tank's ceiling and the final localization is based on the bi-dimensional principle presented above.

In spite of the fact that other authors claim that acoustic waves from the

corroding bottom are spread through the liquid, i.e., bulk waves propagation (Lackner and Tscheliesnig (2003b)), a three-dimensional mathematical approach for locating events has not been proposed in the literature, which opens the door for research.

2.5 Available AE solutions in the main field of application

Over the past decades, technical progresses in the electrical instrumentation field have paved the way to the development of miniaturized and energy efficient instruments for Structural Health Monitoring (SHM). Among the variety of methods used for this purpose, the technique based on acoustic-emission provides a valuable approach not only for the continuous detection of micro and macro changes in the controlled structure subjected to either static or dynamic loads, but also for the localization of the damage itself. In spite of this, AE based monitoring is still far from ubiquitous long-term deployment for several reasons. It is beyond argument that one of the problems is the complexity in the design of the optimal architecture in terms of sensing systems, which is a pillar for the obtainment of high signal-to-noise ratios. However, the deployments cost ultimately determines the demand coverage and it is worth observing that the existing state-of-the-art AE systems are far from being low-cost solutions.

In recent years, companies and academic research groups are striving to develop a new generation of AE systems, tackling some of the limitations towards the implementation of systems for a long-term continuous monitoring, or better known as structural health monitoring (SHM). For instance, Grosse et al. (2008) presented an AE sensor network able to collect acoustic emission data as well as temperature, humidity and strain. The Federal Highway Administration (FHA) and Physical Acoustic Corporation (PAC), two associations affiliated to the MISTRAS group, joined to design a portable AE system designed for continuous outdoor AE monitoring and applied it to several bridges Carlos and Tamutus (2000). Whelan et al. developed an SHM monitoring system for condition assessment, using both accelerometers and strain sensors Whelan et al. (2007). Ferrari et al. (2016) installed a hybrid Wireless Sensor Network (WSN) on the historical Brivio bridge in Bergamo, acquiring acceleration and dynamic displacement response merged by means of a data fusion algorithm. Belisario-Briceño managed to demonstrate that a multi-type sensor network permits the monitoring process to be extended beyond the intrinsic limits of each kind of technology, Belisario-Briceño et al. (2014). Low-cost and small-size sensor nodes networks compliant to the AE phenomena were developed by Wu et al. (2017) and Ledeczi et al. (2009). An integrated structural health monitoring system able

to acquire data from different kind of sensors, including acoustic emissions, was developed and presented in the works of Sagaidak et al. (2014) and Elizarov et al. (2018). Among the several described no one is directly applicable on long term operating sensor, as those needed for SHM purposes, as in order to be applied they require to remove the sensing element from the structure under monitoring. This aspect is a major concern in SHM applications. Yan et al. (2002) designed an innovative AE sensor by integrating a piezoelectric AE sensor to the backing of a conical piezoelectric transducer acting as the transmitter, in order to obtain a self-calibrating AE energy point source. Kober et al. (2016) proposed a reference-free in-situ method of frequency response calibration. This method does not require a specifically designed transducer but exploits the reciprocal calibration and time reversed acoustics (TRA). Moreover, it is not required the detachment of the sensors from the structure to perform the calibration procedure and the method is not dependent on bonding conditions and mechanical properties of the medium. However, the proposed methodology is highly dependent on the conditioning electronic plugged to the transducer, which can affect negatively the measurement.

The analysis of the state-of-art shows that commercial systems developed for this task (structural monitoring via acoustic emission (AE)), Vallen Systeme GmbH, Physical Acoustics (Mistras Group), Softland Times, Sensophone are among the main providers of AE systems, as well as innovative solutions proposed by the academia and research centers, are somehow limited by one or more of the following points:

- bulky equipment which does require a dedicated shelter or on-site storage/control room;
- systems characterized by high-costs, especially because of the number of the high cost transducers which scale with the dimension of monitored structure, space- and power-demanding solutions;
- systems unsuitable to operate outdoor for long time, as they are meant for nondestructive testing (inspections carried out over few hours in ideal conditions) and not for long term monitoring;
- do not allow to measure other physical parameters which could be actually used in a multi-sensing data analysis framework to increase the reliability of the acoustic emission based diagnostic approach;
- absence of embedded self-diagnosis and self-tuning procedures necessary to guarantee the reliability and repeatability, respectively, of the acquired data.

Taking into account the above technological gaps, a global objective of this work is to design and demonstrate an innovative low-cost, low-weight and small-footprint sensor node (SN) with built-in Digital Signal Processing (DSP) functionalities which can yield light and fast deployable sensor networks for long-term and real-time monitoring of acoustic emission (AE) phenomena in storage tanks.

2.6 AE for corrosion and leakage detection

The frequency analysis of corrosion processes and leaks recorded with AE equipment is fundamental knowledge for the designing of the sensitive equipment. For example, work of Martin (2012) notes corrosion observation by AE in the frequency band of around 10 to 80 kHz. In Cho et al. (2006), AEs from the fracture of rusts were successfully monitored by AE sensors of 30 and 50 kHz resonant frequencies, mounted on the terrace of annular plates and the side AST wall. Another example, Prateepasen (2012) demonstrated the controlled pitting corrosion by the potentiostat that applied a constant potential on the specimen where the average frequency of corrosion signals in frequency domain analysis was around 110 kHz. In another example of laboratory pitting experiments, Mazille et al. (1995), the frequency range was mostly 80 to 350 kHz, with a maximum around 160 kHz was observed from the power spectrum calculated using the FFT (fast Fourier transform) of each recorded signal.

The detection of leaks by means of AE in ASTs is little disclosed in the scientific literature. However, according to some publications, the frequency range of this phenomenon belongs to the lower frequencies area compared to corrosion. For example, Morofuji et al. (2003) demonstrated the monitoring of water leakage from the bottom of a tank through an AE sensor with a central resonance frequency of 30 kHz. In literature is also noted that leaks are usually accompanied by continuous AE activity, which makes it difficult to localize it using standard methods based on the time of arrival (ToA) of an AE event. Thus, the boundaries of this work are limited to leak detection, without solving the problem of location.

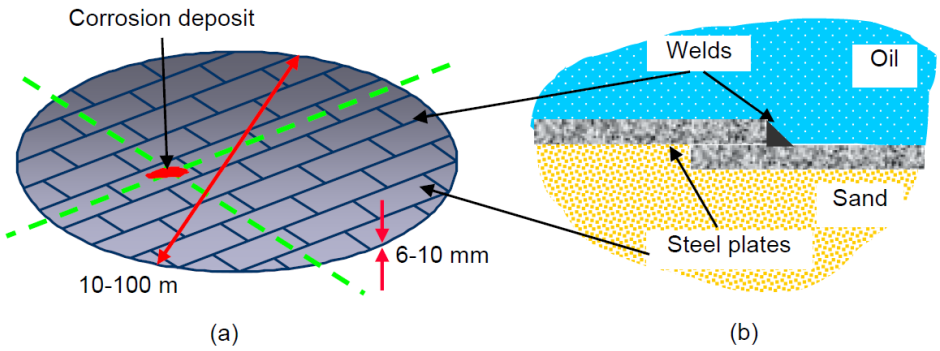

Figure 5: The typical geometry of a tank floor (a) and the model of a lap joint weld (b), Mažeika et al. (2006).

3 Theoretical Framework

Since one of the main objectives of the work is to develop a prototype AE monitoring system, this section reveals the theoretical basis of the developed prototype as applied to the AE phenomenon of corrosion and leakage detection in ASTs.

3.1 The concept of three-dimensional corrosion source location

Acoustic waves propagating from the corrosive deposit are significantly attenuated along the metal sheets on the AST bottom. These energy losses of propagating waves occurs due to the nonuniformity of the tank floor including welds and other inhomogeneities, Mažeika et al. (2006). An example of the overlapping of metal plates on the bottom of the tank is demonstrated in the Figure 5. Therefore, the existing models for bottom corrosion AE source location can take into account bulk acoustic waves propagation in a stored liquid medium, as also stated by Lackner and Tscheliesnig (2003b).

However, as previously discussed in section 2.4, the traditional approach used to locate corrosion source in AST bottoms is considered in two-dimensional space and, accordingly, relatively high localization accuracy can be achieved by reducing the distances between AE sensors (and increasing their number) in one ring placed horizontally along the tank wall. By viewing the tank in three dimensions and adapting the configuration of the AE sensors accordingly, advantages in localization accuracy is supposed to be achieved. Additionally, the proposed approach tends to reduce the total number of sensors which contributes to the overall cost of the final sensor network, a condition which is beneficial for continuous monitoring of storage tanks. A schematic comparison of a bi-dimensional single-ring sensors configuration (yellow dots) and three-dimensional in the form

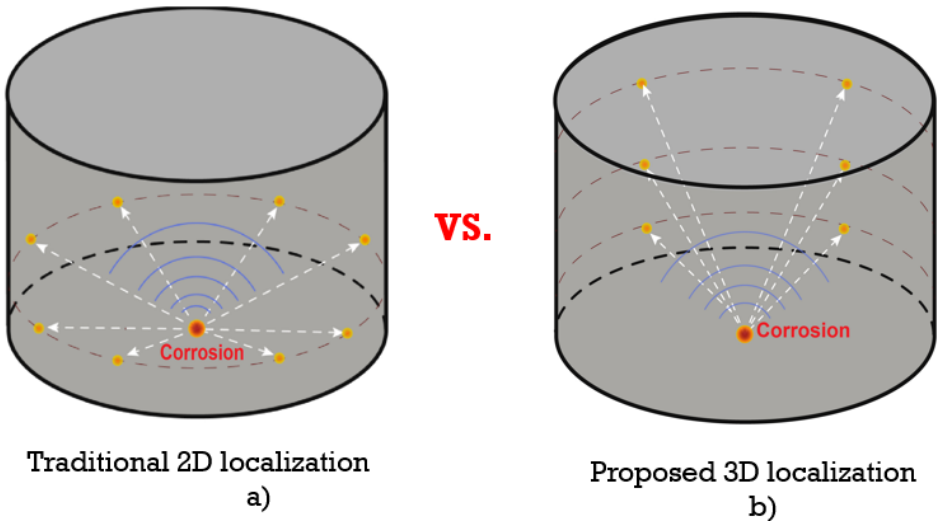

Figure 6: Traditional AE sensors configuration for 2D localization (a) versus the suggested 3D localization (b).

of lines of AE sensors is schematically shown in the Figure 6.

3.2 Functional and technical requirements for the system prototype

Given the previously described peculiarities of corrosion processes and leaks in the AST, as part of this research, a list of requirements for the development of the prototype of AE monitoring system were formulated in Table 1.

It is evident that the technical implementation of an AE monitoring system is multi-step, requiring many competencies such as electronics and microprocessor programming, communication tasks, and the physical fabrication of the prototype. In this study, a stamp-size footprint, low power, and light weight sensor node for impact detection was taken as a starting point for the target development, the architecture of which is described in detail in the work of Testoni et al. (2016).

It should also be noted that additional key points of the research is the methodological organization of testing the developed prototype by simulating the AE phenomenon according to the formulated requirements described in the table 1. Thus, this dissertation intends to reveal non-trivial methods of AE prototype testing, as far as the author knows, never described in the literature.

Table 1: Design requirements for the prototype of AE monitoring system

ID	Requirement	Notes
1	Detection of acoustic emission related to corrosion process	Typical frequency bandwidth between 50 and 350 kHz
2	Detection of acoustic emission related to active leaks	Typical frequency bandwidth between 5 and 50 kHz
3	The difference in the sensitivity to AE-like sources detection of the between prototype and a benchmark AE system shall not exceed 10 dB	The Vallen AMSY-5 AE system has been chosen as benchmark. Verification is required.
4	The accuracy of the corrosion source localization shall not be less than the 10% of the tank diameter	Verification is required
5	The system shall provide a full characterization of the detected AE signals by following features: 1) Rise Time 2) Peak Amplitude 3) Duration 4) AE count 5) AE energy	These features should be extracted locally on the sensor node board. It is required to provide a methodology for checking the correctness of the calculation of these parameters
6	The system shall guarantee continuous monitoring of AE phenomena	Verification is required
7	The system must be able to determine whether the source of noise emission is at the top or at the bottom of the tank.	Verification is required

4 Methodology

This section aims to specify the particular steps has been performed to achieve the research targets, namely the phases development of an AE monitoring prototype as well as the primary experimental campaigns were organised to validate the developed system simulating AE-like events related to the storage tanks. Additionally, the challenges both theoretical and practical that have been overcome, are described in detail.

4.1 Sensor node overview and its validation

4.1.1 Sensor network architecture and sensor node overview

The Smart Sensor Network (SSN), whose interface and sensor architecture were previously presented in the work of Testoni et al. (2016) in detail, is specifically designed to handle continuous monitoring in large-structures. The core of the SSN and the main focus of this work is devoted to the so called piezoelectric 'Sensor Node (SN)', a miniaturized acquisition system able to acquire, pre–process and characterize AE signals for a real-time continuous monitoring. Each device of the network features up to three piezoelectric acquisition channels which passively acquire bulk and/or guided waves originated by impacts, corrosion, or other source phenomena, which travel along the sensorised structure. Up to 64 devices (and 192 transducers) at a time can be connected in a daisy-chain fashion and orchestrated by a network interface (gateway) unit which is describe below. The communication between the main actors of the network relies on a Sensor Area Network (SAN) bus exploiting Data–Over–Power (DoP) communication. In particular, the SAN bus is a sensor bus standard designed to allow microcontrollers and devices to communicate data and power bi-directionally with each other in applications with or without a host computer. It is a half-duplex, single master, message-based protocol, designed to reduce the electrical wiring of general-purpose sensor networks, but can also be used in other contexts. The wires are 120 nominal twisted pair with braid shield. Each node can draw or produce both data and power to or from the bus. The bus is multidrop and the data communication standard is based on EIA RS-485. During acquisition, signals are collected simultaneously by each sensor node.

Gateway

The network interface is built upon a four-building block architecture as shown in Figure 7. An FTDI FT231X USB to full handshake UART integrated circuit (IC) is used to provide USB connectivity for an embedded controller or an external PC (control unit hereafter). The entire USB 2.0 Full Speed protocol is handled

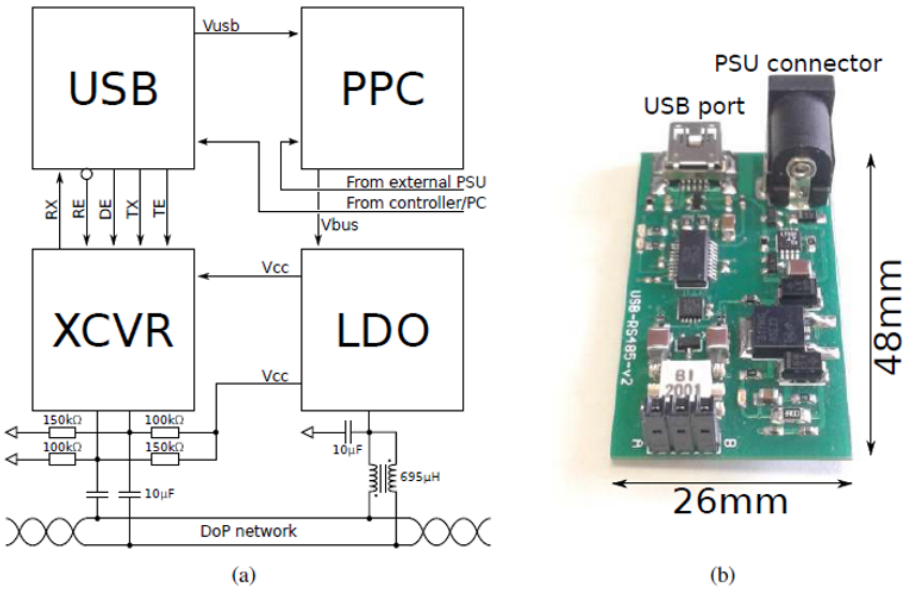

Figure 7: Schematic diagram of the DoP network interface (a) and the gateway interface board (b).

on the chip, allowing for data transfer rates from 300 bps to 3 Mbps at TTL levels.

It is operated by a single supply line taken directly from the USB bus and internally regulated by integrated low-dropout (LDO) regulators. When active, it typically consumes 8 mA, but it can also enter a suspend state in which power consumption drops to125 µA . An industrial temperature range device was chosen to withstand temperatures in the range 40°C to 85°C.

Sensor node

The printed circuit board of the proposed sensor node (shown in Figure 8) is about 30x23 mm wide, consumes less than 40 mA when the bus supply voltage is 5 V, and weighs less than 5 g. Communication to a notebook PC or to an embedded platform like a Raspberry is performed in a half-duplex fashion at an effective speed of 200 ksps by means of a low–voltage, high–speed, half–duplex RS485 transceiver (XCVR). A high–pass capacitive filter made up of purely passive components is used both to interface the transceiver to the DoP bus and to fail–safe polarize the RS485 data lines. A low–pass inductive filter is also present to connect the bus to a low–dropout (LDO) voltage regulator, allowing it to draw power from the DoP network without interfering with data transmission. In particular, a Texas Instrument LM3480 100 mA linear voltage regulator is employed.

The core of the sensor node is the STMicroelecronics STM32F3, a low voltage 32-bit mixed signal microcontroller (MCU) which integrates both Digital Signal

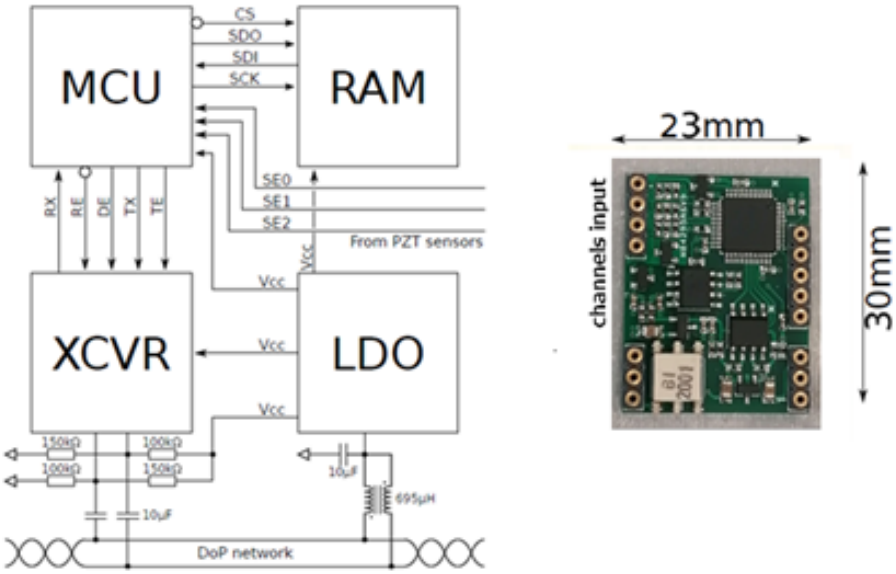

Figure 8: Printed circuit board of the proposed Sensor Node (right) and its architecture (left).

Processing (DSP) and Floating-Point Unit instructions. Moreover, the MCU embeds high precision analog components, such as four Analog to Digital Converters (ADCs) with a resolution up to 12 bit via successive approximation and embedded voltage reference, four rail to rail input/output, low offset voltage Programmable Gain Amplifiers (PGAs) and two 12 bit Digital to Analog Converter (DAC) channels which allow to obtain the maximum output swing. Program instructions and filter coefficients are stored in a 256 KBytes Flash memory embedded within the MCU for the purpose of data pre-processing. After pre-processing, time-domain data are stored in an external 1 Mbit serial SRAM, accessible via Serial Peripheral Interface (SPI) bus. It features a very low power consumption: when in standby mode, only 2 µA are absorbed from the 3.3 V power supply, while operative current is less than 2 mA. An industrial temperature range device was chosen. Moreover, the signal processing capabilities of the node are exploited to allow for AE feature extraction, impact localization and signal characterization, compliant with a complete analysis. Thus, it is possible to perform in real-time and over–time the estimation of several signal features which are usually required by AE testing protocol for damage assessment, such as Peak Amplitude, Rise Time, Duration, Energy, Counts, time of arrival. In terms of signal processing functionalities, the developed AE-prototype is able to collect data in two main modes: (i) recording/transferring mode, including raw data and amplitude-time data and (ii) monitoring mode, performing on-board post-processing by storing AE events in the internal memory and then forwarding them when requested by the PC station.

SHM applications require a minimum level of reliability and accuracy, thus demanding for self-test analysis and calibration procedures. Typically, these procedures are carried out manually by means of expensive bench instruments, resulting to be time consuming and cumbersome. Moreover, in–situ sensor calibration is not always possible, especially in large scale AST scenarios or harsh environments. To overcome these limitations, an innovative tuning procedure purposely designed for the proposed SN prototype and presented in Malatesta et al. (2020). In particular, the capability to perform an automatic tuning procedure without any kind of external bench instrument is demonstrated, allowing for a simplification of the procedure and on–line self–test analysis, speeding up the process. The extraction of the main tuning parameters (such as time constants, voltage biases, time shifts) and their automatic estimation have been embedded within the developed SN firmware.

Aiming for the concept of a cost–effective AE system development, a low-frequency sensor was designed. A coin–size pre–amplifier was embedded directly on each low-cost PZT disk (Murata Piezoelectric Diaphragm) to enhance the sensitivity and the signal–to–noise ratio of the SN acquisition channels whose cost price does not exceed €2 per unit in total. Given the PZT disk resonance frequency is around 2 kHz (see impedance characteristic is illustrated in Figure 10), this solution primarily designed for leakage phenomena detection. The printed circuit board of the pre–amplifier and its protective case are shown in Figure 9. In particular, the circuit is made of three main blocks: a high–gain, common source single stage JFET amplifier with active load, a passive filter and a polarization circuit. The frequency response presents a gain of 19 dB in the bandwidth ranging from 5 kHz to 1 MHz. Moreover, a low noise density of about 31 $\frac{nV}{\sqrt{Hz}}$ at 100 kHz and the low harmonic distortion, with a Spurious Free Dynamic Range (SFDR) computed on the first harmonic of 40 dB, make the preamplifier suitable for high precision AE applications.

Alternatively, SN is compatible with high frequency AE sensors, such as passive (power supply-free) G150 AE sensors, which allow localization of AE events associated with active corrosion on the bottom of storage tanks and other high frequency AE events. G150 operates in the frequency range from 40KHz to 400KHz and with resonant frequency of 150 KHz declared by manufacturer. The AE sensor and it frequency response are presented in Figure 11. A dedicated preamplifier with a gain of 30 dB to interface these sensors to the developed sensor node has been developed and tested as well.

The developed prototype of the AE system deployed on an aluminium plate including a sensor node, three transducers, a gateway, and cables is demonstrated in Figure 12.

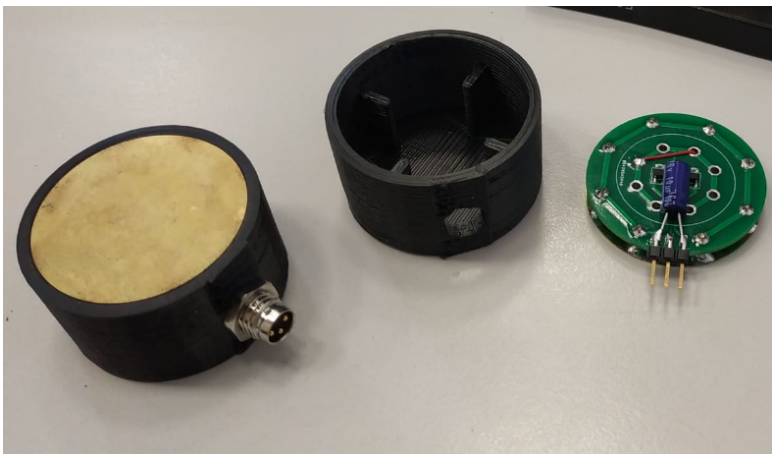

Figure 9: Pre–amplifier on a low–cost PZT disk in a protective case.

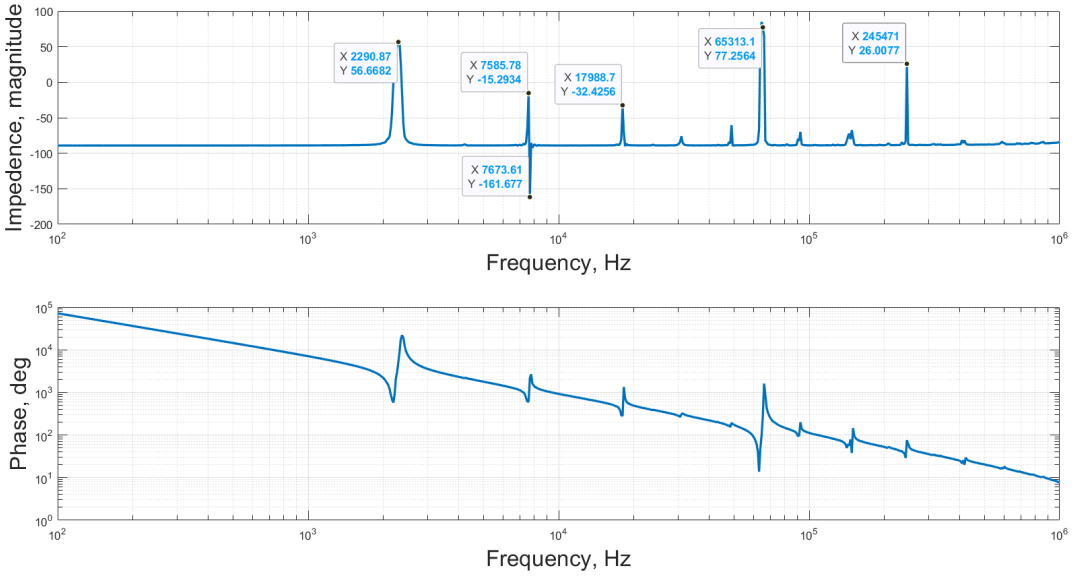

Figure 10: Impedance characteristic of a Murata Piezo Diaphragm 7BB-35-3 obtained by means of Precision Impedance Analyzer (4294A, 40 Hz to 110 MHz).

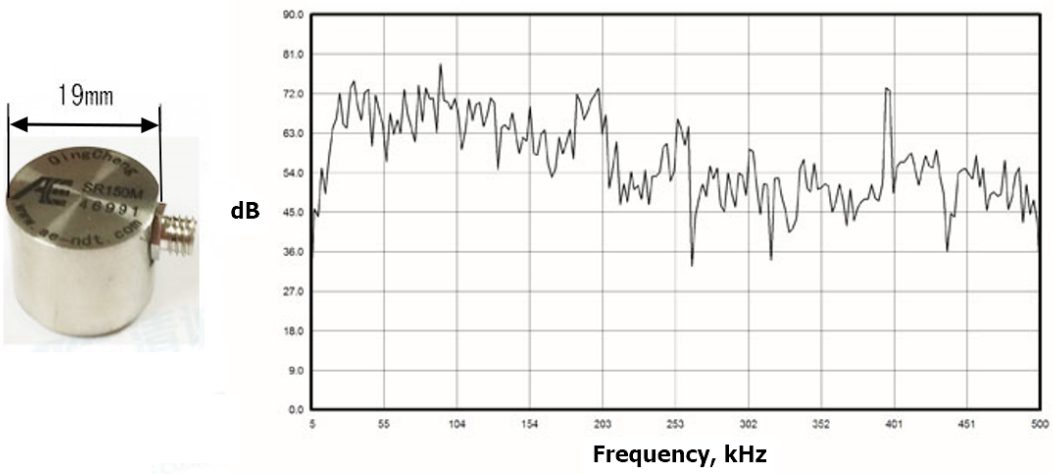

Figure 11: AE sensors G150 (SR150M) and its frequency response.

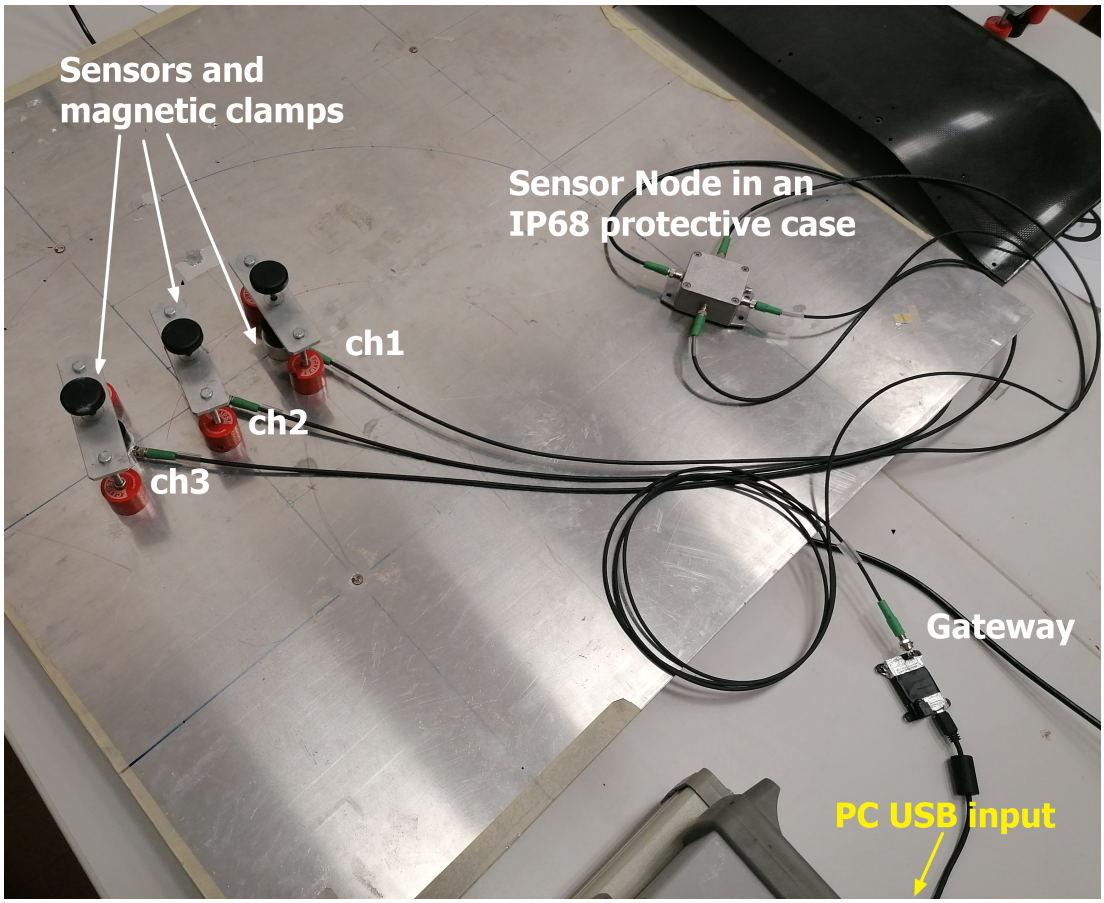

Figure 12: Developed AE systems including a sensor node, three transducers, a gateway and cabling.

4.1.2 On-board signal processing of AE signals

The embedding of AE feature extraction algorithms on the sensor node board has been implemented in compliance with internationally recognized American and Japanese standard practices for AE inspection, such as ASTM (1985), ASTM (2011), for Fiberglass Reinforced Plastic Resin Tanks/Vessels, JIS Z 2342-2002 Mori et al. (2004) for pressure vessels. Therefore, the embedded signal processing capabilities allow to perform several signal features extraction such as Peak Amplitude, Rise Time, Duration, Energy, AE Counts which are schematically indicated in Figure 13. Post–processing of these parameters in turn allows for the computation of additional signal parameters, such as Average Frequency, cumulative representations of Energy, cumulative Hits and cumulative AE count and others which are the key features for damage assessment of various structures under static and dynamic load.

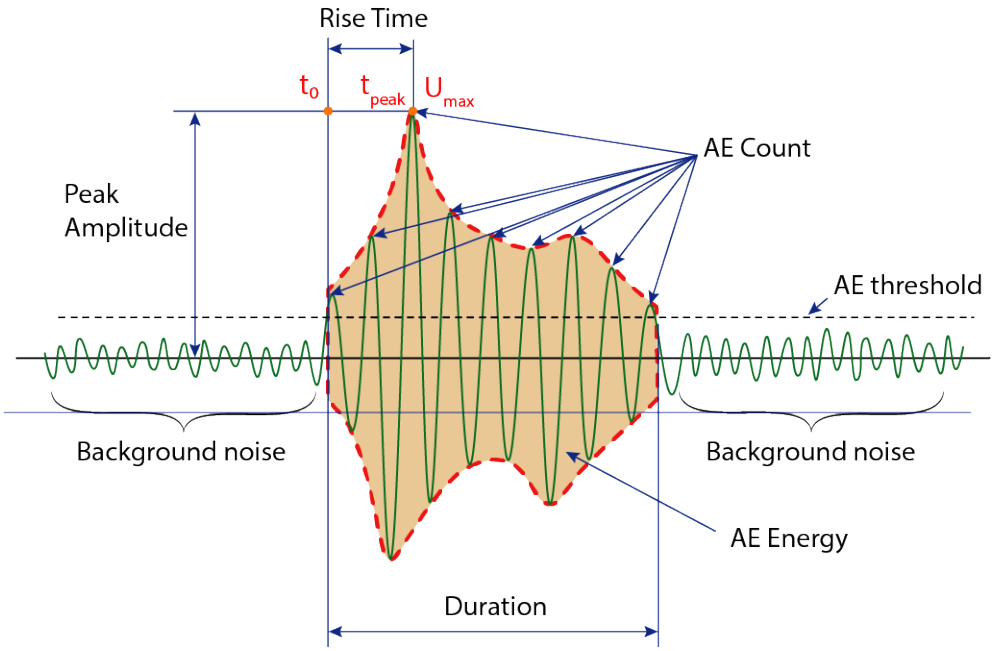

Figure 13: Main acoustic emission signal parameters.

Firstly, triggering event over amplitude threshold is performed. Then basic AE signal features pinpointed in Table 2 need to be estimated which determine the time boundaries of an AE event. For filtering noise-like events, which are usually characterized by high frequency and short duration, a preliminary signal check is performed to exclude unwanted signals for further analysis. Optionally, it is also possible to filter the signal at an earlier stage by the number of threshold crossings between t_0 and t_{end} in accordance with existing practices in the AE field.

The next step of the implemented algorithms is to derive more challenging AE parameters such as peak amplitude in dB relative to 1 µV, rise time in and

Table 2: Basic and principal selected parameters of signal

Feature	Basic selected parameters of AE signal	Unit
t_0	Time of first threshold crossing	[s]
t_{end}	Time of last threshold crossing	[s]
U_{max}	Peak amplitude - maximum signal voltage	[mV]
t_{peak}	Time of maximum signal voltage	[µS]
N_{peak}	Number of threshold crossings between t_0 *and* t_{peak}	[-]
-	**Principal AE signal parameters**	-
t_{AE}	Duration - time between first and last threshold crossing of signal	[µS]
N_{AE}	AE count - number of threshold crossings	[-]
A_{peak}	Peak amplitude, whose calculation formula is given in the equation 1	[dB]
$T_{RiseTime}$	Rise time, whose calculation formula is given in the equation 2	[µS]
E	AE signal energy, whose calculation formula is given in the equation 3	[aJ]

AE signal energy in which are mathematically described in equations 1-3.

$$A_{peak} = 20 \log(\frac{U_{max}}{1\,\mathrm{uV}}) - dB_{amplification} \tag{1}$$

where $dB_{amplification}$ is the overall gain factor in dB.

$$T_{RiseTime} = t_0 - t_{peak} \tag{2}$$

$$E = \int_{t_0}^{t_{end}} U_i^2(t)\, dt \tag{3}$$

where U_i is the signal amplitude value in the time interval from the time of first threshold crossing t_0 to the time end t_{end} of the AE signal under the threshold line.

To correctly carry out the identification of an AE event in amplitude time series (waveforms), it is necessary to distinguish it from any disturbances/noisy spikes that may be perceived at the sensor. In particular, the following identification parameters will be required:

- tbc_MAX is a float variable. Indicates the maximum waiting time that can occur between one crossing of the threshold level (when the signal passes it from above) and the next crossing of the same threshold level (when this is exceeded from below). The value must be expressed in ms.

- tae_min is a float variable. Indicates the minimum duration that the recorded oscillation can be considered as an AE event. Spike noises can

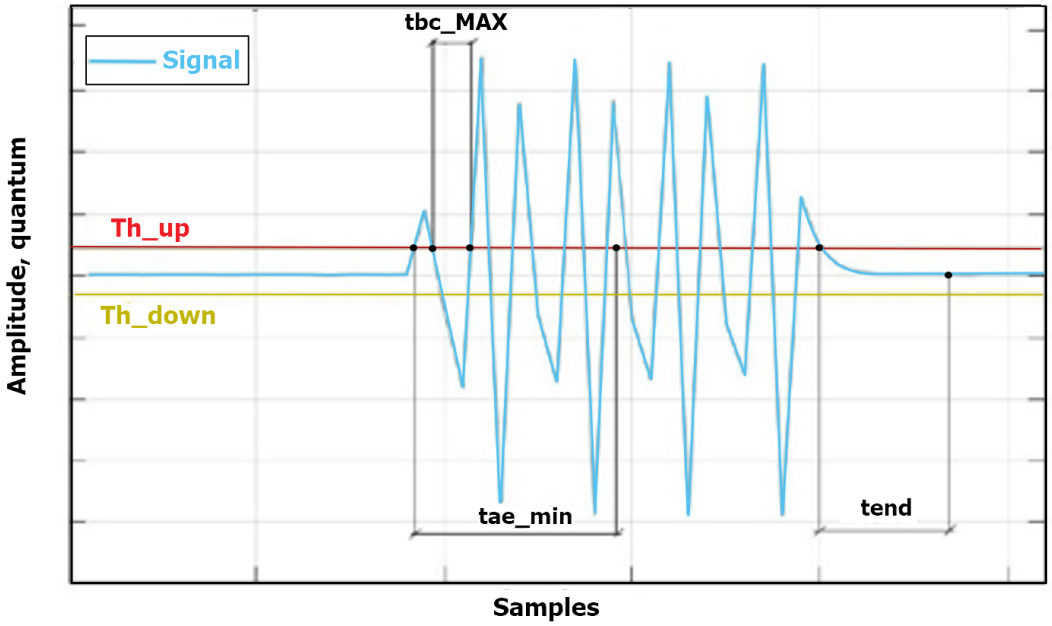

Figure 14: Display of fundamental parameters of AE signal selection.

be filtered out at this stage. The value must be expressed in ms.

- tend is a float variable. Indicates the minimum time that must elapse in which the signal is below the threshold level to consider the identified AE terminated. The value must be expressed in ms.
- data_ch is an array of data acquired by a one among 3 channels of sensor node.
- Th_up is a variable of type int. It contains the value of the upper threshold level set by the User. It is calibrated considering the noise in the surrounding environment.
- Th_down is an int variable and contains the value of the lower threshold level set by the user. set by the User. It is calibrated considering the noise in the surrounding environment.

An example of the AE signal selection is presented in the Figure 14. The entire logical sequence of the AE features extraction algorithm detailed in Appendix A.

4.1.3 Metrological validation of the algorithm

After embedding the algorithms into the sensor node, a preliminary validation phase was performed. A schematic diagram of the employed equipment and the relative connections are depicted in the Figure 15. Such a scheme involves the

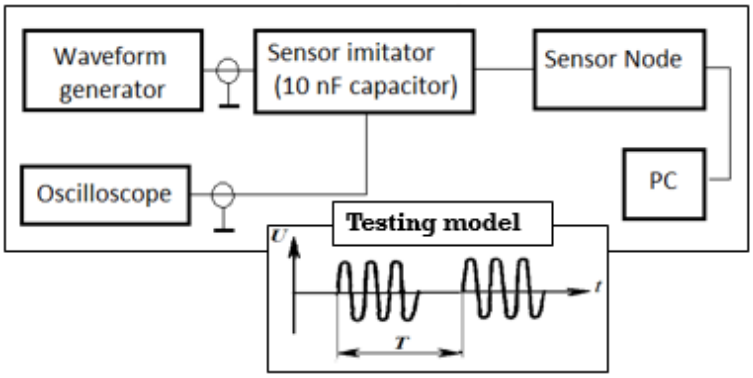

Figure 15: Equipment connection diagram to test AE features processed on–board.

Table 3: Build-in algorithm verification

AE feature	Mathematically estimated	Computed in SN	Absolute error
Peak Value, dB	123.52	123.71	0.19
Duration, ms	0.2	0.2	0
Energy, aJ	97.6405	99.69	2.05
Counts	20	21	1

use of radio pulse type signals consisting of a sinusoidal burst packages as simulation of AE events, whose amplitudes, repetition periods, and duration are set with high precision by the AWG Agilent 33250. The number of preset sinusoids in one burst also allowed for a reliable check of the AE count crossing threshold. A Digital Oscilloscope (Tektronix PDO 3014) was used as a control signal instrument. Moreover, a 10 nF capacitor was exploited as the electrical equivalent of a piezoelectric sensor typically connected to the developed SN. Test signal parameters were chosen as follows: i) sinusoidal burst frequency – 100 kHz, ii) peak signal amplitude – 1.5 V (or 3 V peak-to-peak), iii) burst duration – 20 cycles (equivalent to 200 µs of duration at a frequency of 100 kHz). A sample rate of 500 kHz was chosen to gather data in a time window of 1 ms. After manual triggering of the signals raw waveforms together with on–board processed AE features were transferred from the SN to the PC through a companion gateway device for subsequent verification. The main results comparing the correspondence of built-in algorithms with their theoretical expectations as described in Figure 13 are provided in Table 3.

4.1.4 Laboratory experimental validation

The main objective of the experimental campaign were (*i*) testing the developed prototype of AE system both in terms of sensitivity to different materials used in the industry, and (*ii*) assessing the performances in a relatively long-term

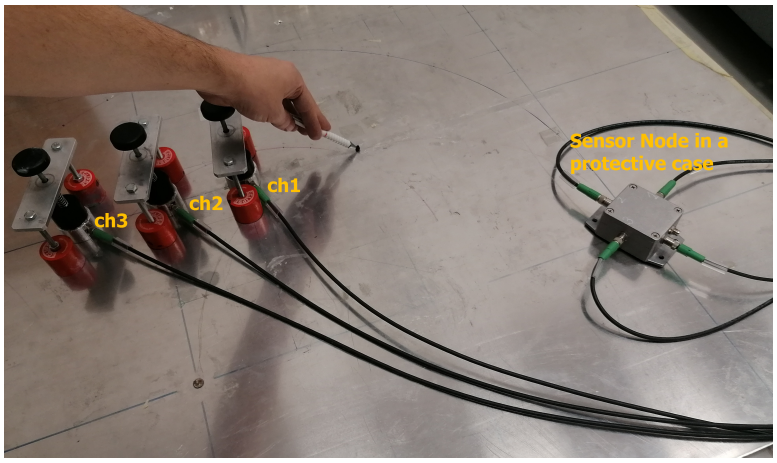

Figure 16: Hsu-Nielsen test on an aluminium plate.

monitoring regime close to *in situ* conditions. The results of the successful test of the prototype development are published in a Ph.D candidate work, Bogomolov et al. (2021b).

As far as the material test was considered, two sample 1000 mm x 1000 mm square plates with thickness of 3 mm were exploited, the first one made of aluminum and the second one being a carbon fiber material. The widely known Hsu-Nielsen method (pencil lead break) described in the work of Teodorczyk (2017) was used as the excitation source for wide–band frequency acoustic events. Three transducers with built-in pre–amplifiers were arranged in lines, each sensor 10 cm apart from the others, and then a pencil lead break test was performed 10 cm far from the transducer of channel 1 (see Figure 16). With the help of magnetic sensor holders and magnets on the back of the plate, the transducers were tightly pressed to the surface. A similar approach was endorsed for the carbon fiber plate.

During the long–term monitoring phase, AE activity of real scenarios was simulated. To this end, a great number of authors, as for instance provided by Johnson et al. (2012), Pullin et al. (2010), Krampikowska A (2019) and Rivera et al. (2018), note the high dependence between the development of dangerous defects as cracks or corrosion with significant growth in intensity of trends of acoustic emission parameters such as AE count, Energy, Hits, and in some cases Peak Amplitudes. Thus, the experimental setup was built to simulate the defect evolution condition and check the response of the developed AE prototype during a 4-hour continuous monitoring test. As schematically shown in Figure 17, three transducers/channels of a sensor node were deployed on the carbon fiber plate at distance of 10 cm in between. Furthermore, a piezoelectric disk of the buzzer-emitter was also attached to the surface of the plate at a distance of 35 cm using adhesive tape. To excite the buzzer-emitter, the leads of its PZT disk were

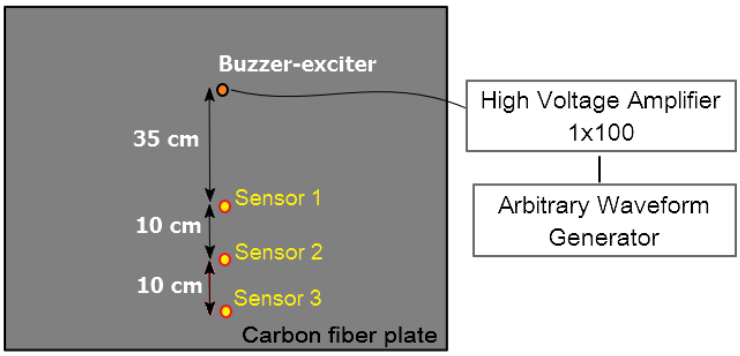

Figure 17: Testing scheme of sensor node in monitoring mode on a carbon fiber plate.

Table 4: AWG settings over 4 hour test

Period	**Period between burst packages, s**	**Amplitudes, mV (output of AWG)**
1st hour	30	300
2nd hour	15	400
3rd hour	10	500
4th hour	1	600

connected to the output of a Tegam high voltage amplifier (model 2350) which amplified signal from the Arbitrary Waveform Generator (AWG) Agilent 33250 with an amplification factor of 100.

As in the preliminary tests, the radio pulse type signals consisting of a sinusoidal burst package were used, whose amplitude and repetition period were dynamically adjusted in compliance with most common signs of defect development used in long-term AE monitoring (structure transition from less stressed to more stressed state), keeping other output signal's parameters as constants. Thus, by setting the frequency to 70 kHz and selecting 5 cycles of sinusoid in one burst package as constant values, the period between burst packages, T, and its amplitudes, A, were changed every hour as it described in Table 4.

Among the settings of the sensor node, the sampling frequency was set to 200 kHz, the sampling length was equal to 5000 samples, the triggering time to 500 samples and the built-in amplifier level was chosen 0 since the distance between the buzzer-emitter and the transducers was relatively small. To visualize the data in real time, the system was configured to send every second to a connected laptop the parameters of the post-processed data. The configuration was carried out in the MATLAB environment.

Results pertaining to the sensitivity tests are presented in Figures 18-19. As can be seen, the signal amplitude in the case of aluminum sheet reaches about 400 mV peak-to-peak, whereas for the carbon fiber plate almost 1 V peak-to-

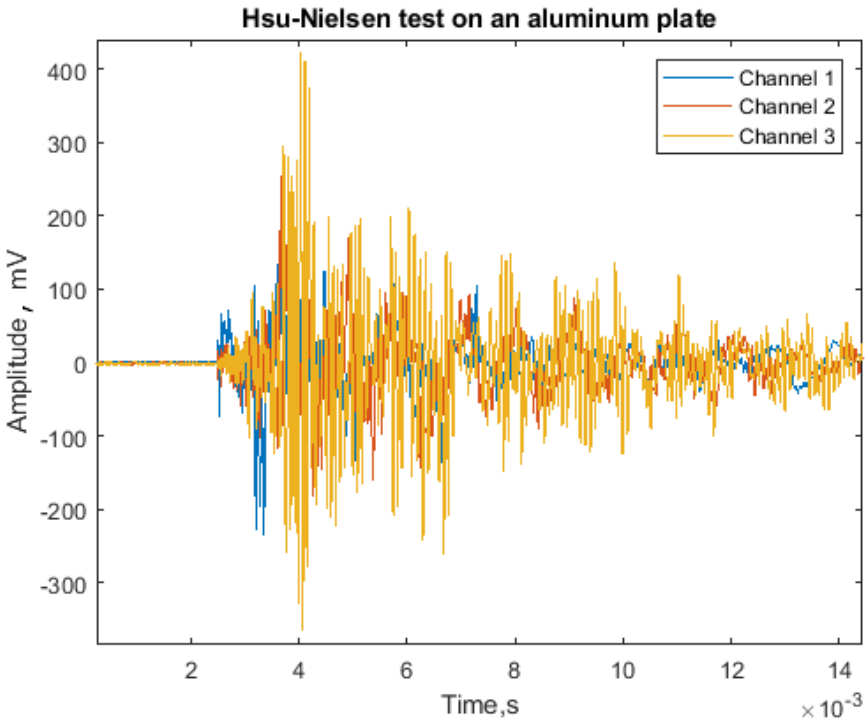

Figure 18: Waveform recorded in SN due to Hsu-Nielsen test on an aluminum plate.

peak was measured, which are confident signal w.r.t. operational signal-to-noise ratio. Undoubtedly, this preliminary confirmed that even low–cost piezoelectric buzzer discs can be employed as an possible alternative solution to commercial AE transducers.

The results of the second phase of the experimental campaign, are shown in Figure 20. In particular, left plot of Figure 20 shows the Count, Energy, and Hits parameters coming from the sensor node were converted to cumulative form in the post-processing stage on a PC to perform a deeper analysis of the recorded AE trends. The vertical axis was represented in a logarithmic form for greater informativeness due to the large number of recorded AE events within 4 hours. As can be seen, especially from the cumulative count trend, the value of this parameter grows every hour on a logarithmic scale. Substantial growth of all cumulative curves upwards during the last fourth hour of monitoring is due to the 10-fold increase in the central frequency of the mechanical excitation of the signal, making the transition from a period of 10 s to 1 s. The cumulative AE Hits trend, in turn, demonstrates the that all the three channels of the developed system recorded the same number of events which is explained by the close distance between the transducers. Another group of parameters such as Peak Amplitude, Rise Time and Duration versus monitoring time are presented as scatter plots on right side of Figure 20. In this specific case, the Peak Amplitude trend better

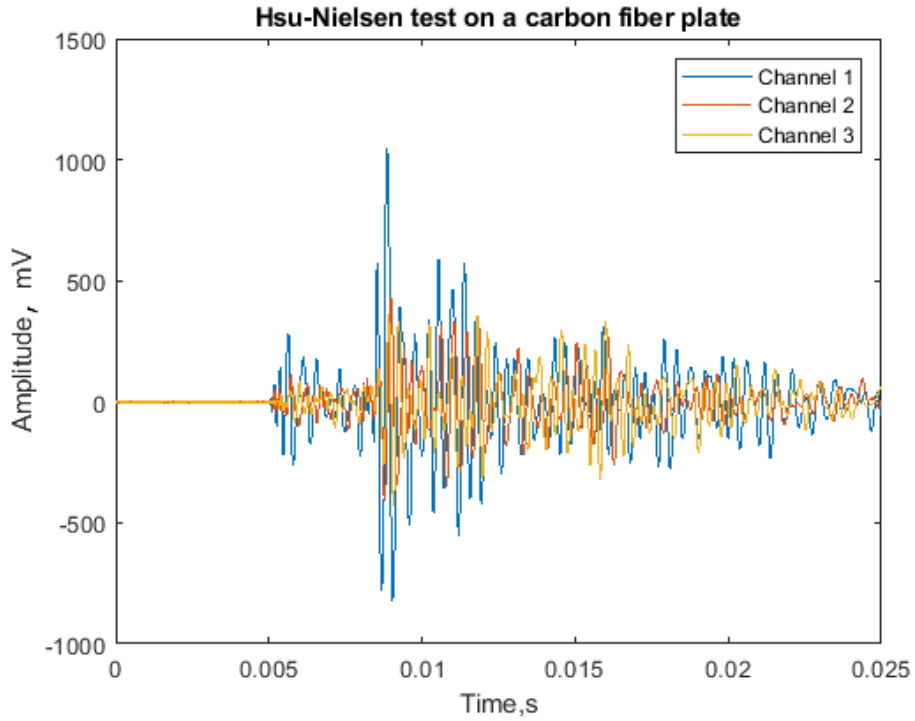

Figure 19: Waveform recorded in SN due to Hsu-Nielsen test on a carbon fiber plate.

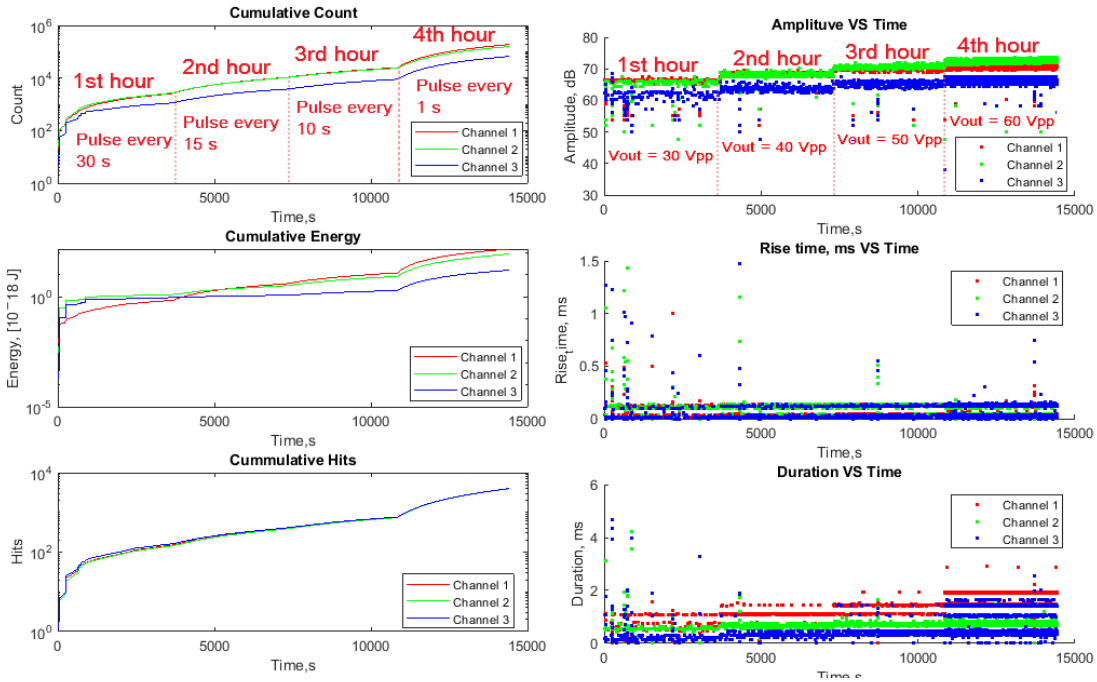

Figure 20: 4 hours monitoring test on carbon fiber plate: *i*) AE count, energy and hits in cumulative representation on the left graph and AE *ii*) amplitude, rise time and duration on the right.

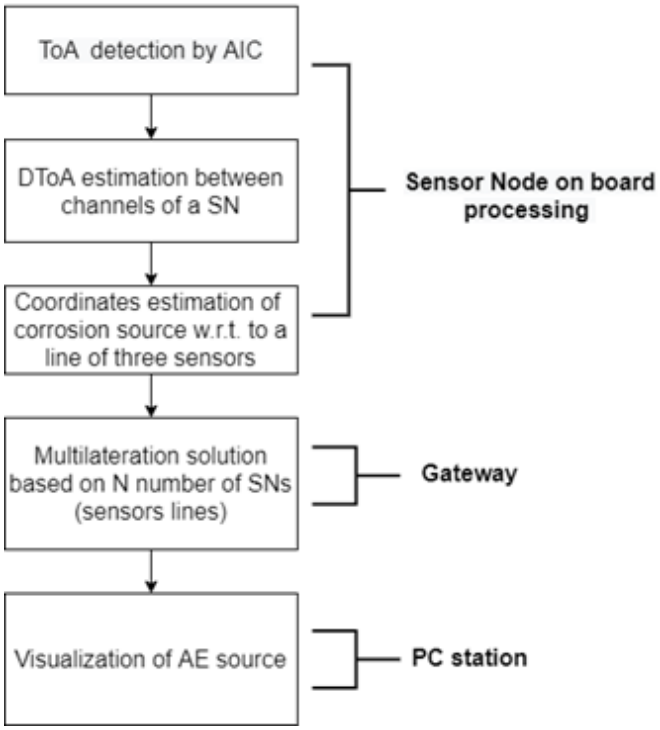

Figure 21: Localization Algorithm Diagram.

captured the increase in the signal content by measuring a variation of about 1-2 dB associated with stepwise changes of the amplitude. The gradual extension of the Duration of the selected area of processing signals over a fixed threshold amplitude also occurs due to the hourly increase in the amplitude of mechanical displacement thereby slightly distancing the start, t_{start} and end, t_{end} of a triggered AE events from each other.

4.2 Three-dimensional localization solution

4.2.1 Technological aspects of AST bottom corrosion localization

The developed prototype of AE system with high-frequency G150 AE sensors allows localization of AE events associated with active corrosion at the bottom of storage tanks. The basic idea of corrosion localization is based on four basic steps (see schematically Figure 21): 1) AE time of arrival detection by means of the Akaike Information Criterion (AIC) on every channel of a sensor node unit; 2) estimation of time difference of arrival (DToA) between three AE channels) estimation the distance/coordinates between the vertical position of a three sensors line and the corrosion source 4) the summing up of the corrosion coordinates from multiple number of sensors lines (multiple SNs) by solving the multilateration problem on a gateway board. The data visualization can be organized at a remote PC station.

Solutions of mathematical challenges related to corrosion localization steps are disclosed in the following subsections.

4.2.2 Onset signal estimation

Time of arrival estimation (or onset time determination) of a transient signal is extremely important in AE applications, since it directly results in the accuracy of event location and source mechanism analysis. The true ToA of an AE event could be described as the moment when the first energy of a particular signal phase reaches the sensor positions. In the signal analysis, the onset time is usually picked as the point where the first difference between the signal and the noise takes place Kurz et al. (2005). It is necessary to have reliable automatic picking tools, because human analysts cannot manage the vast amount of data recorded in the whole monitoring process. Thus, various algorithms have been proposed for automatic detection of onset times. Most of the methods are coming originally from the seismological science, since seismology and AE measurement are similar fields in terms of signal processing point of view. The simplest form for ToA detection is to use an amplitude threshold-picker Tong and Kennett (1996). In this method, some special value is set for amplitude of signal as the threshold, and the onset time is determined as the time when the value of the corresponding amplitude exceeds the threshold value. However, the result from this method is very rough and sometimes is not available for a pure threshold approach, such as small amplitude signals and/or signals with a high noise level. Another approach using a dynamic threshold is the so-called STA/LTA (STA – Short Term Average, LTA – Long Term Average) picker by Carpinteri et al. (2012). This approach assumes that the STA measures the instantaneous signal amplitude, while the LTA contains information about the current average acoustic noise amplitude. With the same idea, various forms of STA/LTA are defined. But due to the fact that the useful signal and noise of acoustic emission are often in the same frequency range, the STA/LTA picker does not give sufficiently accurate results Carpinteri et al. (2012).

To cope with these issues, Akaike Information Criterion (AIC) approaches the task of ToA identification as a pure statistical problem based on the second order statistics of the measured acoustic data. In essence, AIC leverages the concept of signal entropy to detect abrupt changes in the statistical distribution of the observed signal (y St-Onge (2011), Pearson et al. (2017)). For a discrete signal with N samples, this is achieved by computing, for each sample k, the quantity:

$$\mathrm{AIC}[k] = k \log \sigma^2_{y[1:k]} + (N - k - 1) \log \sigma^2_{y[k+1:N]} \tag{4}$$

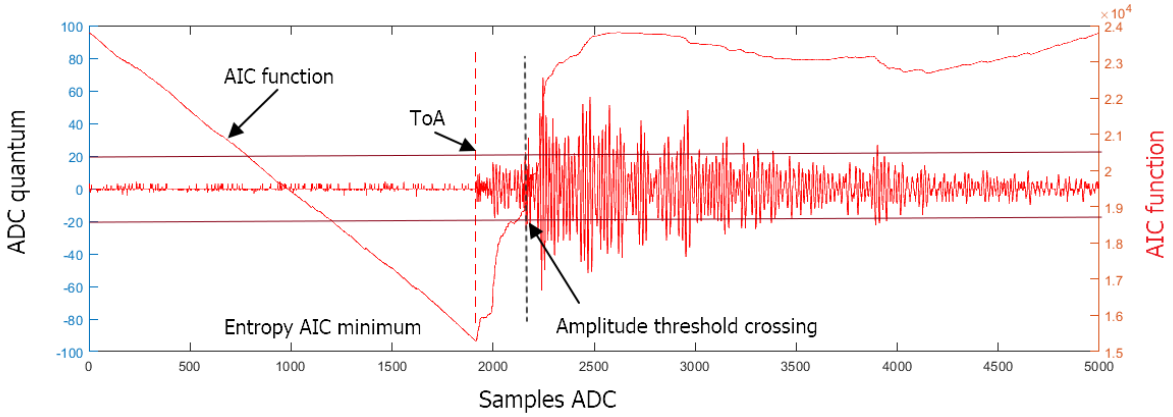

Figure 22: Akaike Information Criterion for ToA signal estimation.

which is a logarithmic measure of the cumulative variance (σ_y^2) of the preceding ($y[1:k]$) and successive ($y[k+1:N]$) signal window with respect to the current sample index k. In other words, AIC splits the full waveform into a k dimensional and an $N-k$ dimensional smaller vector, respectively spanned by the first N and the last $N-k$ samples, and describes the level of similarity between them. The demonstration of the superiority of the AIC over a traditional crossing of the amplitude threshold to detect ToA is shown in Figure 22.

The rationale is that, in correspondence of a sharp change in the signal profile, such as the one associated with the arrival of the incoming wave–front generated by the acoustic source, the divergence between the two variances increases to a large extent, generating a minimum in the overall AIC function. The instant of time aligned with this minimum is the sought ToA, Pearson et al. (2017).

Notably, this method can provide reliable outcomes when the processed signal presents two clearly distinct regions, e.g., an high–entropy portion where uncorrelated noise dominates, and a low–entropy segment where the acoustic signal is present (Li et al. (2017)). To be implemented in the FLASH memory of the developed sensor node, the signal is primarily processed by the built-in high-pass filter in order to obtain the cleanest possible signal at the input of the AIC algorithm.

To verify the AIC processing for AST application, the propagation of elastic waves generated by an AE departing from the center of the bottom surface of a 95 cm radius tank filled by water up an height of 90 cm was simulated in COMSOL Multiphysics software. The description of the FEM simulations is out of the scope of this thesis. The radial displacements taken on the tank wall at 91 equally spaced points, at heights from 0 to 90 cm, where recorded with a sampling frequency of 100 kHz and up-sampled by means of interpolation to a sampling frequency of 2 MHz. Each acquired amplitude time series was processed according to the algorithm described above in the text.

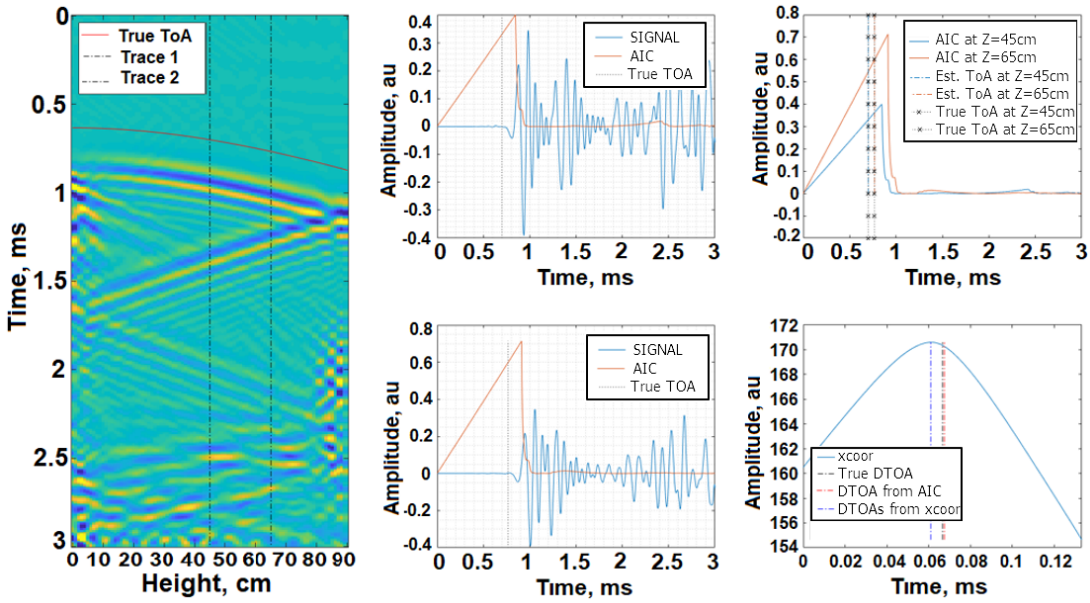

Figure 23: Results of the AIC estimation process on simulated amplitude time series.

The test bench interface shown in Figure 23 has been realized. On the left panel a collective representation of all the collected time waveform from 0 to 90 cm is shown, where two dash dotted lines highlight the position of two different signal traces which are shown in the others panel of Figure 10. In particular, each amplitude time series, along with the computed AIC and the true Time of Arrival (ToA) of the elastic wave is shown in the central column. A constant offset is usually present between the peak of the AIC (original entropy function is inverted w.r.t. Figure 22 for better visualization) and the true ToA: this offset is removed by the optimization process. The results of the optimization process are shown on the right column, where a comparison between the true ToA, the estimated ToA and each AIC is shown on the top panel. On the bottom panel, the cross-correlation between the computed AICs is shown: superimposed to this curve are plotted the true Difference in ToA (DToA) between the two traces, and the DToA estimated from the AIC peaks difference and the cross-correlation peak. The estimation of the DToA through the AIC peak difference is expected to be more accurate than the cross-correlation result since AIC is a maximum likelihood estimation of the ToA.

Some alternative approaches for ToAs estimation based on advanced neural networks algorithms have been studied and presented the article of Zonzini et al. (2022) in more detail. The PhD candidate contributed to this work by designing the experimental set up, conduct the measurements, labeling the dataset and analysing the results.

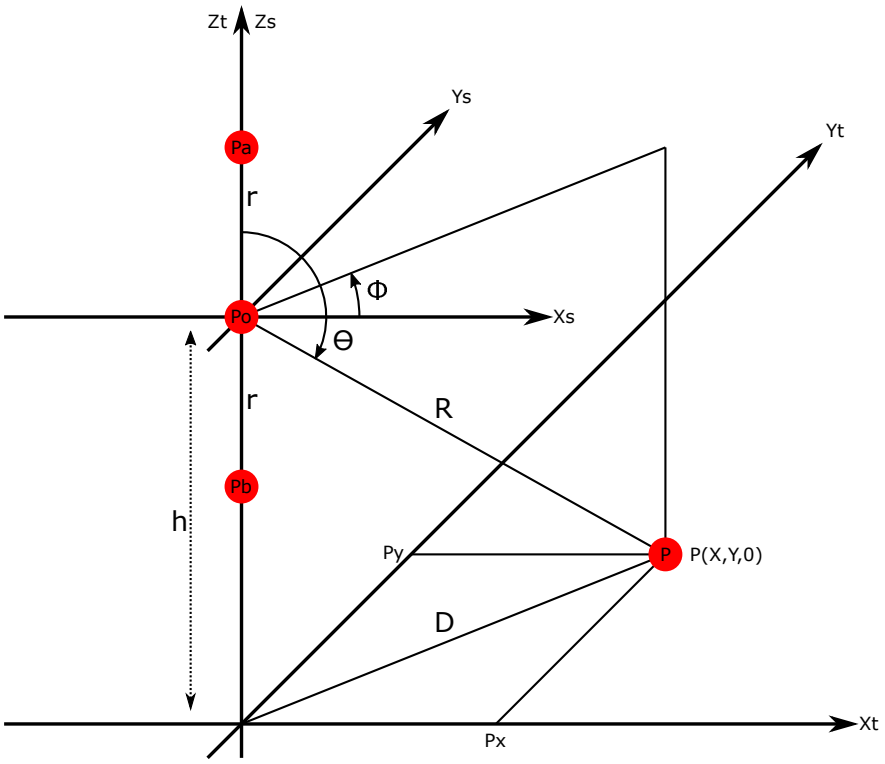

Figure 24: Sensing element arrangement (Po, Pa, Pb) for the estimation of the distance D separating an acoustic emission source point P from the sensing elements vertical image.

4.2.3 Mathematical solution for AST bottom source location

The algorithms to locate an AE source for two possible different sensors arrangements ("vertical line" and "star") to be placed on the outer walls of the tank are discussed. The sensing elements arrangement of the "vertical line" can be parameterized by means of two parameters: h, the height of a reference sensing element Po and r, the distance between the reference element Po and each of the satellite elements Pa and Pb (see Figure 24). Once the signal originated by the AE has been collected by each sensing elements Po, Pa, and Pb, the collected amplitude time series are pre–processed and the time of arrival at each collection point are estimated as already discussed.

If the speed v of the elastic wave originated by the AE is not known, it is possible to estimate it by applying the following formula:

$$v = r f_s \sqrt{\frac{1 - \frac{N_b}{N_a} - \frac{2h}{r}\frac{N_a+N_b}{N_a}}{N_b(N_b - N_a)}} \tag{5}$$

where N_a and N_b correspond to the difference in samples between Time of Arrivals (ToAs) computed on the amplitude time series acquired by the reference element Po and the one by Pa and Pb respectively, and fs is the sampling frequency of the sensor node. Once v is known, it is possible to estimate the travel distances

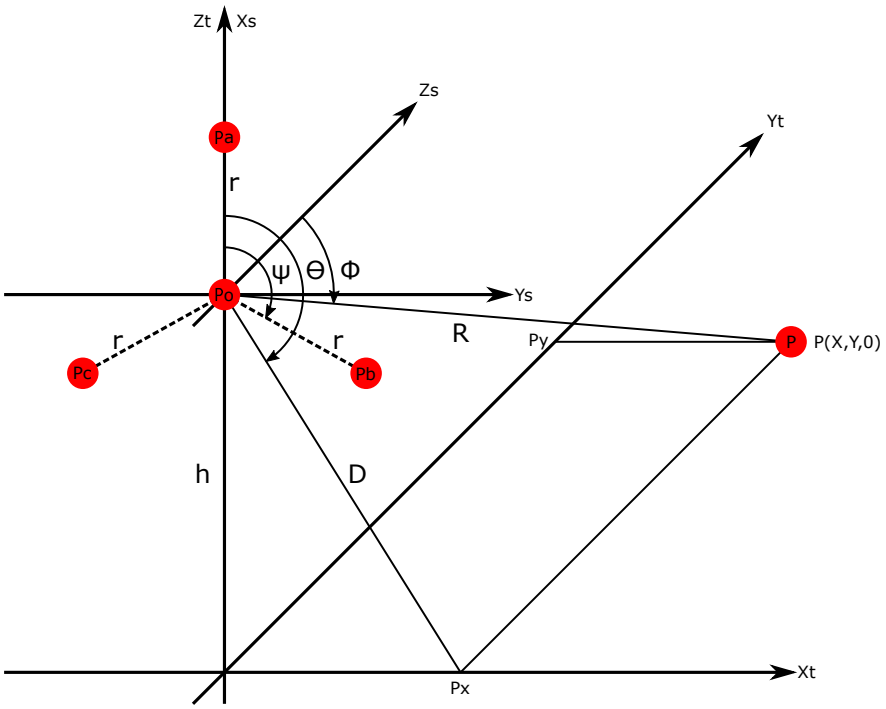

Figure 25: Sensing element arrangement (Po,Pa,Pb,Pc) for the estimation of the XY position of an acoustic emission source point P with respect to the sensing elements vertical image.

$\Delta_{a,b}$ as $N_{a,b}$*v / fs. Then, it is possible to compute the radial distance D as:

$$D = \frac{h}{x} \cdot \sqrt{1 - x^2} \tag{6}$$

where x is defined as:

$$x = \frac{h\Delta_a}{r^2 + 2rh - \Delta_a^2} + \frac{h\Delta_b}{r^2 - 2rh - \Delta_b^2} \tag{7}$$

Once the radial distance D has been estimated by each sensor node, the XY position of the AE source on the bottom of the tank can be estimated by means of multilateration algorithms which will be described later in the text.

It is possible to strengthen this estimation by adopting the "star" sensing element arrangement as illustrated in Figure 25. This more complex sensing element arrangement, in addition to h and r, is characterized by a third parameter Ψ which represent the angular separation of the satellite elements Pb and Pc with respect to the reference pair Po-Pa. Once the signal originated by the AE has been collected by each sensing element Po, Pa, and Pb, the collected amplitude time series are pre-processed and the time of arrival at each collection point are estimated as already discussed.

If the speed v of the elastic wave originated by the AE is not known, it is possible to estimate by applying the following formula:

$$v = r f_s \sqrt{2 \frac{\left(1 + \frac{2h}{r}\cos(\psi)\right) - \left(1 + \frac{2h}{r}\right)\frac{N_b + N_c}{2N_a}}{N_b(N_b - N_a) + N_c(N_c - N_a)}} \tag{8}$$

where N_a, N_b and N_c correspond to the difference in samples between the ToAs computed on the amplitude time series acquired by the reference element Po and the one by Pa, Pb, and Pc, respectively, and fs is the sampling frequency of the SN. Once v is known, it is possible to estimate the travel distances $\Delta_{a,b,c}$ as $N_{a,b,c}$*v / fs. Then, it is possible to compute the XY coordinates as:

$$\begin{cases} R = \dfrac{h}{x} \\ X = R \cdot y \\ Y = R \cdot \sqrt{1 - x^2 - y^2} \end{cases} \tag{9}$$

where x and y are defined as:

$$\begin{cases} x = \dfrac{2h\Delta_a}{r^2 + 2rh - \Delta_a^2} \\ y = \dfrac{\Delta_c - \Delta_b}{2r\sin(\psi)} \left(1 + \dfrac{x}{2} \cdot \dfrac{\Delta_b + \Delta_c}{h}\right) \end{cases} \tag{10}$$

To verify the distance estimation algorithm the test bench interface shown in Figure 26 has been realized. The same simulation dataset as described in 4.2.2 was exploited. On the top row, the three amplitude time series collected respectively at Po, Pa, and Pb are shown, along with the computed AIC and the representation of the true and estimated ToA. On the bottom part of the interface, a scale representation of the tank is present. On the right side, the three sensing elements Po, Pa, and Pb are shown: their position is defined by the height h=30 cm of the reference element Po and the distance r=10 cm between each of the satellite elements Pa, Pb and the reference element. The simulated AE location is shown as a black dot, whereas the estimated AE location is shown as a yellow dot: it is possible to appreciate the estimation error.

Once the rough estimate of the XY position of the AE on the bottom of the tank has been computed by each sensor node, the final XY position of the AE on the bottom of the tank can be estimated by means of multilateration algorithms.

4.2.4 Multilateration Algorithm

This category of algorithms is well known in literature Norrdine (2015) and many efficient implementations exist, also for devices with limited computational resources. As depicted in Figure 27, the goal of these algorithms is to estimate the position (x', y') of an unknown point given the positions (x_i, y_i) of N fixed sensing

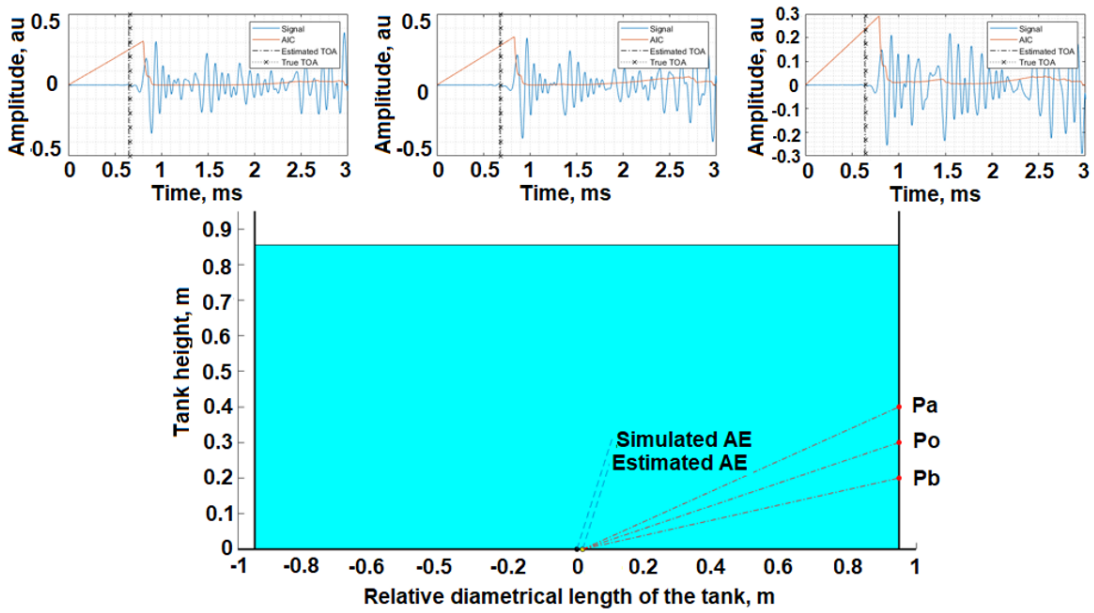

Figure 26: Results of the distance estimation process on simulated amplitude time series.

devices and a set of radial distances d_i from each these points to the unknown point.

Many algorithms exist to solve this problem: generally speaking, for each pair of distance and position the following equation can be written:

$$(x_i - x')^2 + (y_i - y')^2 = d_i^2 \tag{11}$$

Collecting all the equations and subtracting from the Nth each of the first N-1 yields the following equation set:

$$\begin{cases} 2(x_N - x_1)x' + 2(y_N - y_1)y' = (d_1^2 - d_N^2) - (x_1^2 - x_N^2) - (y_1^2 - y_N^2) \\ \vdots \\ 2(x_N - x_{N-1})x' + 2(y_N - y_{N-1})y' = (d_{N-1}^2 - d_N^2) - (x_{N-1}^2 - x_N^2) - (y_{N-1}^2 - y_N^2) \end{cases} \tag{12}$$

which can be rewritten in a matrix form as:

$$2\begin{bmatrix} (x_N - x_1) & (y_N - y_1) \\ \vdots & \vdots \\ (x_N - x_{N-1}) & (y_N - y_{N-1}) \end{bmatrix} \begin{bmatrix} x' \\ y' \end{bmatrix} = \begin{bmatrix} (d_1^2 - d_N^2) - (x_1^2 - x_N^2) - (y_1^2 - y_N^2) \\ \vdots \\ (d_{N-1}^2 - d_N^2) - (x_{N-1}^2 - x_N^2) - (y_{N-1}^2 - y_N^2) \end{bmatrix} \tag{13}$$

Since the number of sensing points is usually greater than 3 to improve the robustness of the estimation, the previous matrix equation represents an over determined system. In such cases an optimal solution can be computed by min-

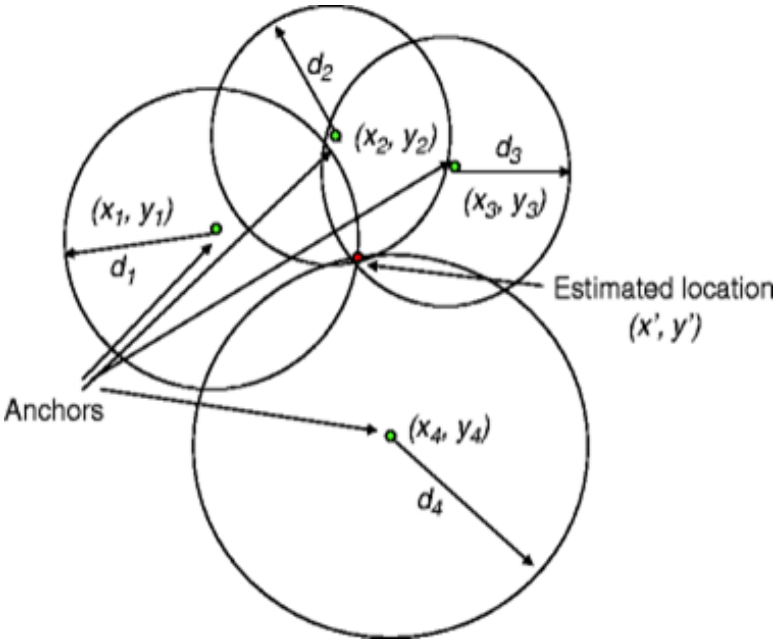

Figure 27: Generic setup of multilateration algorithms.

imizing the mean square error $||\mathrm{Ax}-\mathrm{b}||^2$ where $A/2$ is the left-hand matrix, b is the right-hand vector and x is the vector of the unknown coordinates. An optimal solution to this problem is the well known pseudo inverse matrix which results in the solution $\hat{x} = (A^T A)^{-1} A^T b$. Thus, the projection of p on the column space of A is:

$$p = A(A^T A)^{-1} A^T b \tag{14}$$

The desired coordinates of p on the column space $\mathrm{Col}(A)$ represent the solution $\hat{x}$.

In the practical case, where the reference points lie on the some plane (the storage tank bottom), the solution is given by

$$x = x_p + t x_h \tag{15}$$

where x_p is a particular solution of $A_0 x = b_0$ and x_h is a solution of the homogeneous system $A_0 x = 0$, i.e. x_h is a Basis of $\mathrm{Kern}(A_0)$. The free real parameter t is calculated by minimizing the quality factor d. The vectors x_p and x_h can be computed using the Gaussian elimination method. The particular solution x_p can also be determined using the pseudo inverse of the matrix A_0. The pseudo-inverse gives the solution with the minimum norm $A_0 x = b_0$.

Summarizing the mathematical derivations and limitation outlined in Nordine (2015), the solutions of the equation system $A_0 x = b_0$ are

$$\begin{cases} x_1 = x_p + t_1 x_h \\ x_2 = x_p + t_2 x_h \end{cases} \tag{16}$$

Solutions of the multilateration problem are the points: $N_1 = x_1\ I$ and $N_2 = x_2 I$, where

$$I = \begin{vmatrix} 0 & 0 & 0 & 0 \\ 0 & 1 & 0 & 0 \\ 0 & 0 & 1 & 0 \\ 0 & 0 & 0 & 1 \end{vmatrix} \tag{17}$$

5 Empirical Results

This section summarizes the key results of experimental studies aimed at validating the developed prototype of the AE system, as well as the proposed model of three-dimensional location both on a small tank built in a laboratory and on a real water storage tank. Part of the test description pays special attention to controlled AE simulation methods with instrumentation in the context of AST bottom has not yet been proposed in the literature.

5.1 Sensor Node verification on a small-scaled storage tank

To simulate the target conditions, the developed AE prototype was tested in a specifically built small–scaled storage tank (see photo in Figure 28) placed in a laboratory of University of Bologna. The storage tank features 1900 mm of diameter, 950 mm of height. The main objectives of the tests were to study the waves propagating in the tank both from below and from above, simulating condensate flowing off the roof of a real tank, as well as to organize trial location algorithm verification. Additionally, the sensitivity test of the developed prototype in comparison with a commercial AE Vallen systeme deployed their sensors on the tank's wall was performed.

Figure 28: Small-scaled storage tank.

5.1.1 3D location algorithm test

To test the location algorithm, three vertical lines of three G150 AE sensors each were disposed every 120 degrees along the tank circumference, which for sake of clarity will be called as line 1, line 2 and line 3. To excite the bulk waves

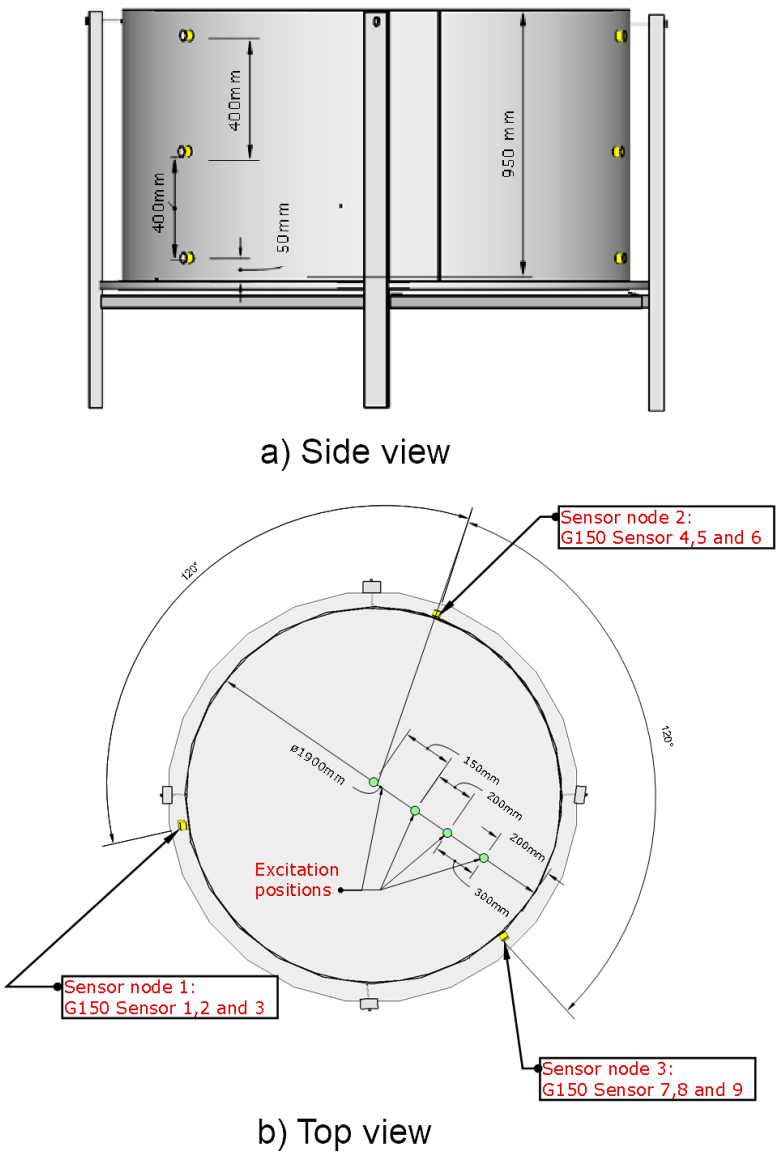

Figure 29: Sensors deployed on the small storage tank, a) top view and b) side view.

propagating in water, as a simulation of the waves emitted by an evolving bottom corrosion, an immersed insulated buzzer disk (Murata Piezoelectric Diaphragm) was exploited. The buzzer was placed on 4 different positions at the bottom of the tank. The radial distance between the targets lines and SN 3 is equal to 10 cm or 6 degrees (line projection from the center to the tank wall). The sensors layout and the excitation positions are depicted in Figure 29.

For better visualization, an example of the operation of the location algorithm for target 1 (central point) is shown in Figure 30.

The results of the experiment are presented in Table 5. The average absolute location error was estimated at about 15 cm.

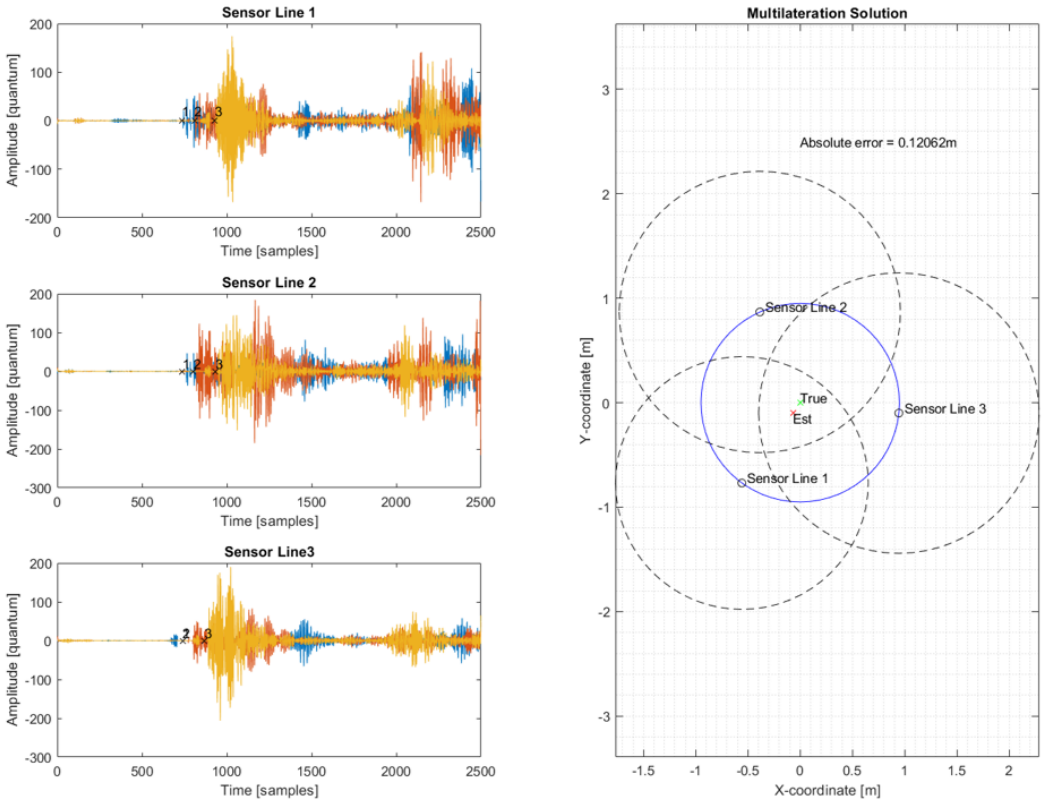

Figure 30: Localization of target 1.

Table 5: Location test results

	Position	Absolute error, cm
target 1	Center of the tank	12
target 2	0,15 m from the middle of the tank	19
target 3	0,35 m from the middle of the tank	3
target 4	0,65 m from the middle of the tank	27

5.1.2 Comparative amplitude-frequency test

An important technical aspect affecting the ability to detect a useful signal from the waves spreading from the corrosion source on the tank bottom is the sensitivity of the system in a wide range of frequencies. Consequently, a comparative evaluation of the frequency response of the developed prototype was performed using the a commercial Vallen acoustic emission system as a benchmark which it is known to be used for tank inspection. As in the previous experiment, the waves excitation source was stimulated from inside the small tank filled with water by means of the PZT diaphragm insulated electrically from water.

For the prototype, a G150 AE sensor was used whereas for the Vallen system, three different sensors were deployed. The G150 AE sensor of e-siam system was connected to a dedicated designed 26 dB-preamplifier (plus 10 dB internal gain of the sensor node), while Vallen's VS- 150M AE sensor was plugged to Vallen's AEP5 34 dB preamplifier whereas the other two Vallen sensors, namely VS150-RIC and VS75-SIC, are equipped with built-in 34 dB preamplifiers. In both systems the sampling frequency of the acquisition was set to 1 MHz. The excitation signal generated by the Arbitrary Waveform Generator (AWG) Agilent 33220A was amplified with a Power Amplifier GA 2500A with about 300 Vpp signal output sent to the PZT actuator. An oscilloscope, Tektronix DP03014, was plugged to the output of Power Amplifier to control the output linearity of the signal. A coil of coaxial cable with a length of 80 meters was used for its preliminary testing before testing on a real tank where this cable length will be justified by the size of the experimental setup. The diagram and photo of the test are shown below in Figure 31 and Figure 32 respectively.

To test the frequency response, a set of excitation frequencies was chosen according to the metrology E6 standard logarithmic progression from 4.7 to 470 kHz. A signal-to-noise ratios (SNRs) estimation for all sensors of the two AE systems was performed. TThe resulting SNRs were evaluated in MATLAB (SNR function) by estimating the power spectral density (PSD) of a central waveform frequency sampled at 1 MHz. The curves derived from the SNR algorithm are compared in Figure 33. These results demonstrate comparable sensitivity performance of the two systems to within a few dB over the entire frequency range.

5.1.3 Simulation of condensate droplets

The water-drop droplets tests was performed in order to investigate the capabilities of the Sensor Nodes to detect events similar to the drops of condensate from the ceiling of a real size tank. Such events usually cause false AE events and should be filtered out in post-processing. A hose attached to a wooden rod

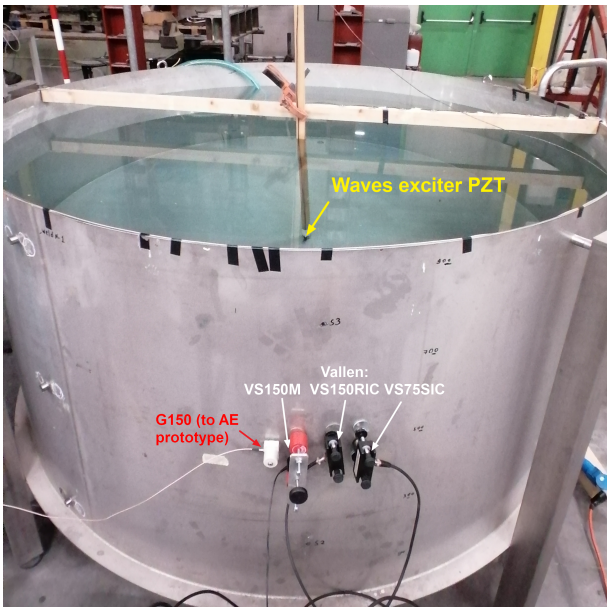

Figure 31: Photo of sensor deployment of two AE systems for sensitivity test.

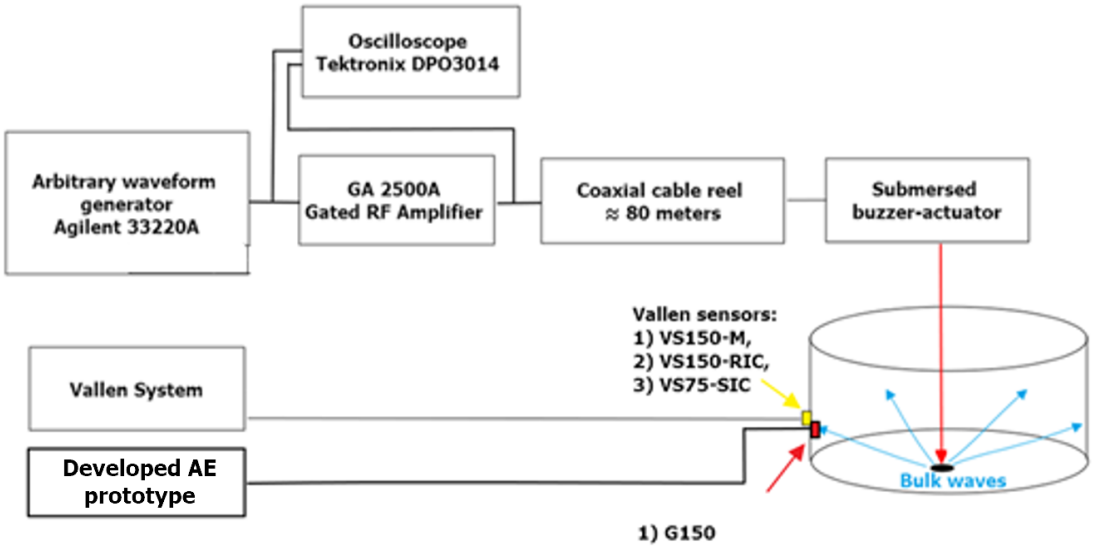

Figure 32: Experimental setup for testing the sensitivity of an developed AE prototype using Vallen system as a benchmark.

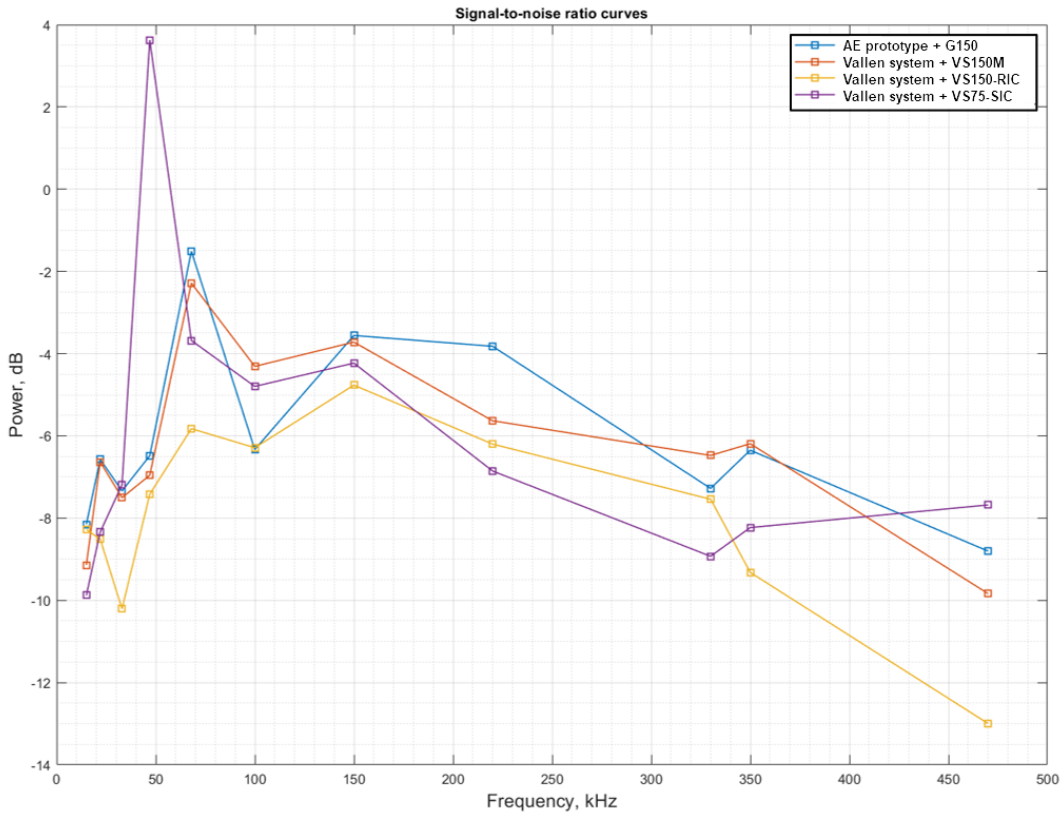

Figure 33: Signal to noise ratios analysis.

was attached 1 meter above the tank to squeeze water into the center of the tank from a medical syringe attached to the other end of the hose. The configuration of sensor positions was remained as depicted in Figure 29, but only one line of three G150 sensors was exploited.

As demonstrated in Figure 34 (on the right), the droplets were detected by the system, clearly showing the order of waves originating first from the upper sensor AE and approaching the lower sensor with the greatest time delay. The schematic view of the experiment and ToAs estemated on recorded waveforms are shown in Figure 34 (left and right, respectively).

5.2 Sensor Node verification on a real storage tank

5.2.1 Induced leakage test

Induced leakage tests were organized to probe the developed AE prototype. In particular, the objectives of the experimental camping were (i) to detect the leakage and (ii) to estimate the minimum detectable leakage. As such different leakage scenario were realized by changing the amount of leakage. During the leakages the raw AE waveforms were collected (recording/transferring mode) for the purposes of characterizing the type of structural damage. In addition, AE pa-

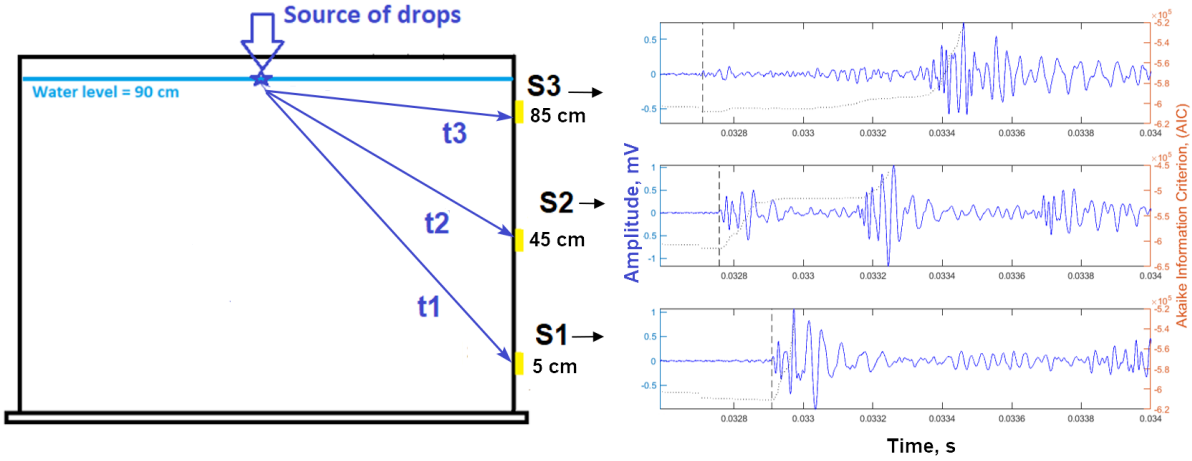

Figure 34: Schematic positioning of sensors on the scaled storage tank and expected flight time from droplet-induced AE source (S1-S3 sensing probes and t1-t3 Time of Arrival of S1-S3).

Table 6: Leak quantification

nozzle [mm]	**experimental results [lt/sec]**	**leakage [lt/h]**
1	1.5 litres per 241.6 sec	22.35
2	1.5 litres per 57.5 sec	93.92
3	5 litres per 88.9 sec	202.47
4	5 litres per 51.3 sec	350.87
5	5 litres per 32.8 sec	548.78
6	5 litres per 22.1 sec	814.47
7	5 litres per 15.5 sec	1161
8	5 litres per 11 sec	1565.2
9	5 litres per 9.5 sec	1894.7

rameters computed automatically on the SN (monitoring mode) were transmitted in real time to the remote PC for further analyses.

To validate the effectiveness of the proposed SN to monitor leakage a 17 m high and 18 m in diameter, filled with water to a level of about 6.2 m, located in one of the Eni S.p.A. storage parks (Voltaggio, Italy), was considered and an experimental campaign was designed (see the Figure 36). To stimulate leakage, a drain valve positioned at the outer bottom side of the water tank, was used. The valve position in spatial relation to the position of the line of three transducers is shown in the schematic of Figure 35. To consider different leakages, nine nozzles with diameters ranging from 1 mm to 9 mm and a step of 1 mm were manufactured to be connected to the drainage valve (see Figure 37). The loss of stored media (water) in litres for the nine nozzles was measured connecting them one by one to the considered drainage valve. Results are reported in Table 6.

The sensor node (SN) and three piezo diaphragm transducers were mounted

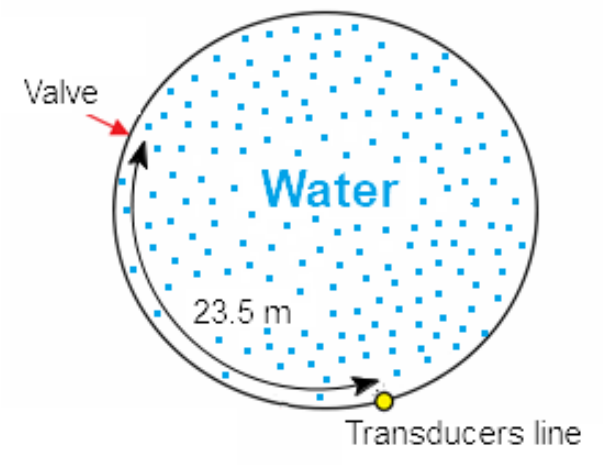

Figure 35: Schematic arrangement of valve and transducers on the storage tank, top view.

Figure 36: Storage tank and schematic water level.

Figure 37: Nozzles with holes of various diameters.

on the tank. In particular, the tank surface was cleaned, ultrasonic gel was used as a couplant, and three diaphragm-based transducers were mounted and kept in position using magnetic holders as shown in Figure 38. The three sensors were connected to the SN, hold in its protective case specifically made for long term monitoring on site conditions, also kept in position via magnetic holders. The position of the sensors bonded on the tank with respect the drainage valve is shown schematically in Figure 35.

To establish the minimum size of induced leakage that could be detected by the developed AE system the considered valve was equipped with the different nozzles and the leakages were monitored. AE features, processed directly on-board of the SN, were transferred to PC station for final visualization and recordings.

Leakage characterization.

At first, raw time waveforms were recorded and analyzed. The periodograms of some recorded signals for closed and open valve, shown in Figure 39, demonstrates the presence of a high energy component at 1.19 kHz for the open valve case. No evidence of high energy components above 20 kHz (upper bound of the plots in Fig. 39) was found.

60 seconds monitoring.

After, to establish the minimum amount of leakage that could be detected by the developed AE monitoring prototype, leakage was monitored by recording AE events, extracting AE features and collecting their trends while nozzles from 1 to 9 mm holes were used.

Figure 40, for instance, shows the distributions of the Peak Amplitude for the AE recorded from the different nozzles during a monitoring phase of 60 seconds. From the histograms and their Poisson distribution (red curves) with an alpha tolerance of 95 %, no clear statistical difference can be observed. Similar statistical analysis was performed for the Duration and Rise Time of the same AE events. A clear pattern indicating a relationship between these parameters and

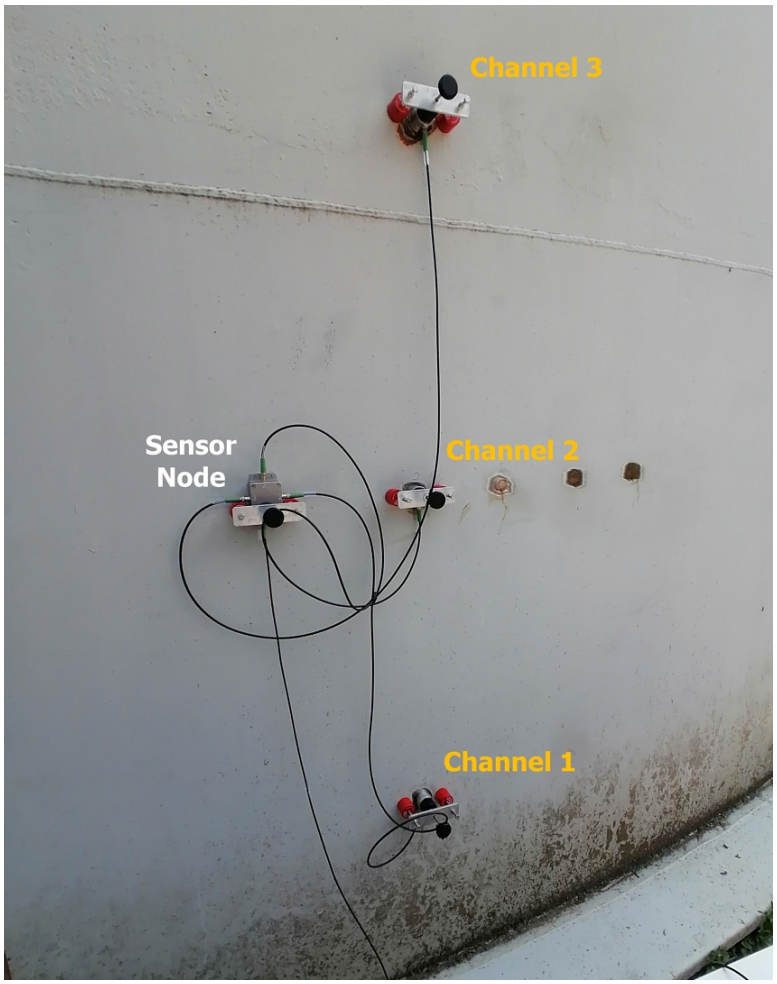

Figure 38: Placement of the Sensor Node in a protective case and transducers on the wall of the tank.

the leak size was not observed.

Figure 41 shows for the same 60 seconds of monitoring the Cumulative Counts, the Cumulative Energy and the Cumulative Hits of the AE. As it can be observed from the Hit and Count trends, the leakage diameter has some influence on the slope of the curve, in particular with an 8 mm nozzle the trend grows more than for the other ones. However, it is worth noting that at low values of orifices (1-3 mm) the increase in these parameters is also significant, with cumulative energy of AE signals increasing even more rapidly than in the case of 7-9 mm nozzles. Another interesting observation is the intensive growth of cumulative energy for leaks of 2, 3 and 4 mm, with a subsequent decay after about 30 seconds, while other leaks are characterised by more uniform trends.

These involved patterns, possibly related to the complex wave propagation phenomena inside the tank, even if do not allow a neat characterization of the nozzle dimension, denote clearly the capability of the developed system to detect AE due to the leakage. The key results of this experiment are published in the

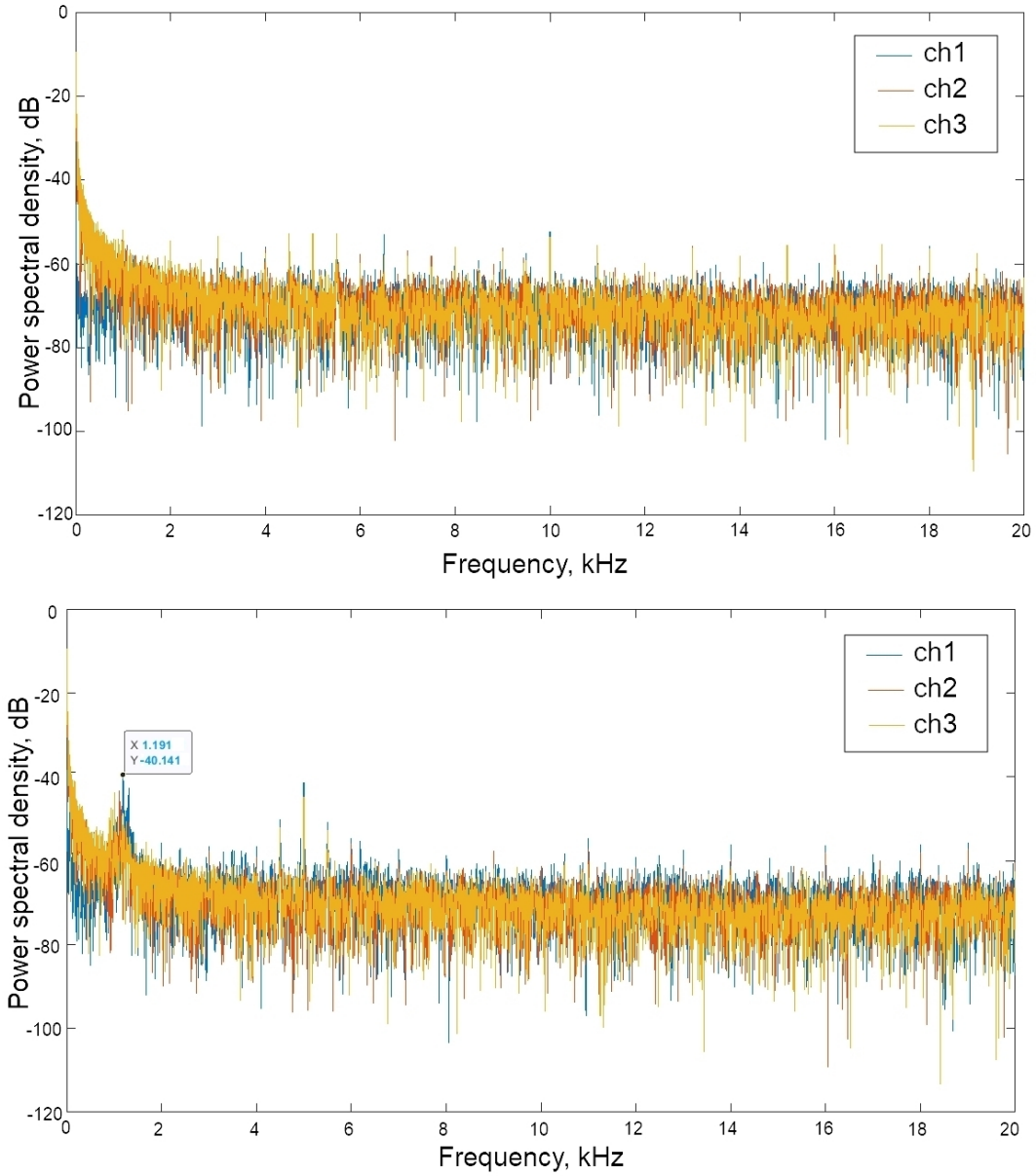

Figure 39: Periodograms of the signals while no leakage, valve closed (top) and during active leakage, valve open (bottom), nozzle 4 mm.

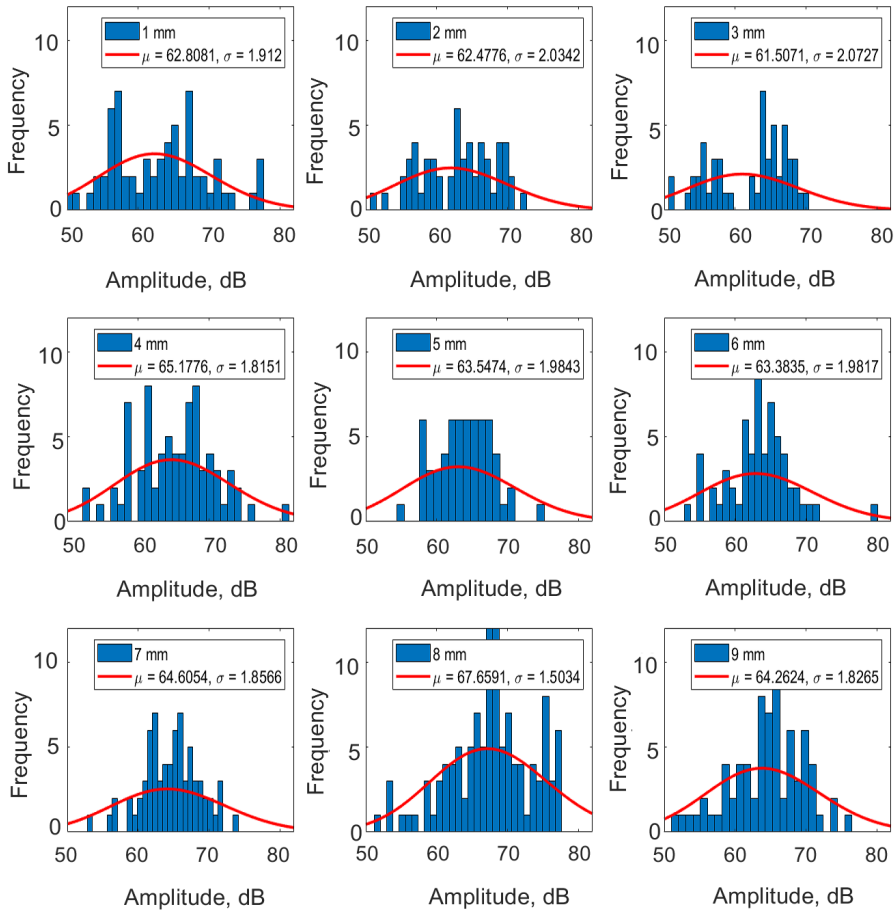

Figure 40: Histograms of Peak Amplitude distribution with reference to leakage size for 60 seconds of monitoring.

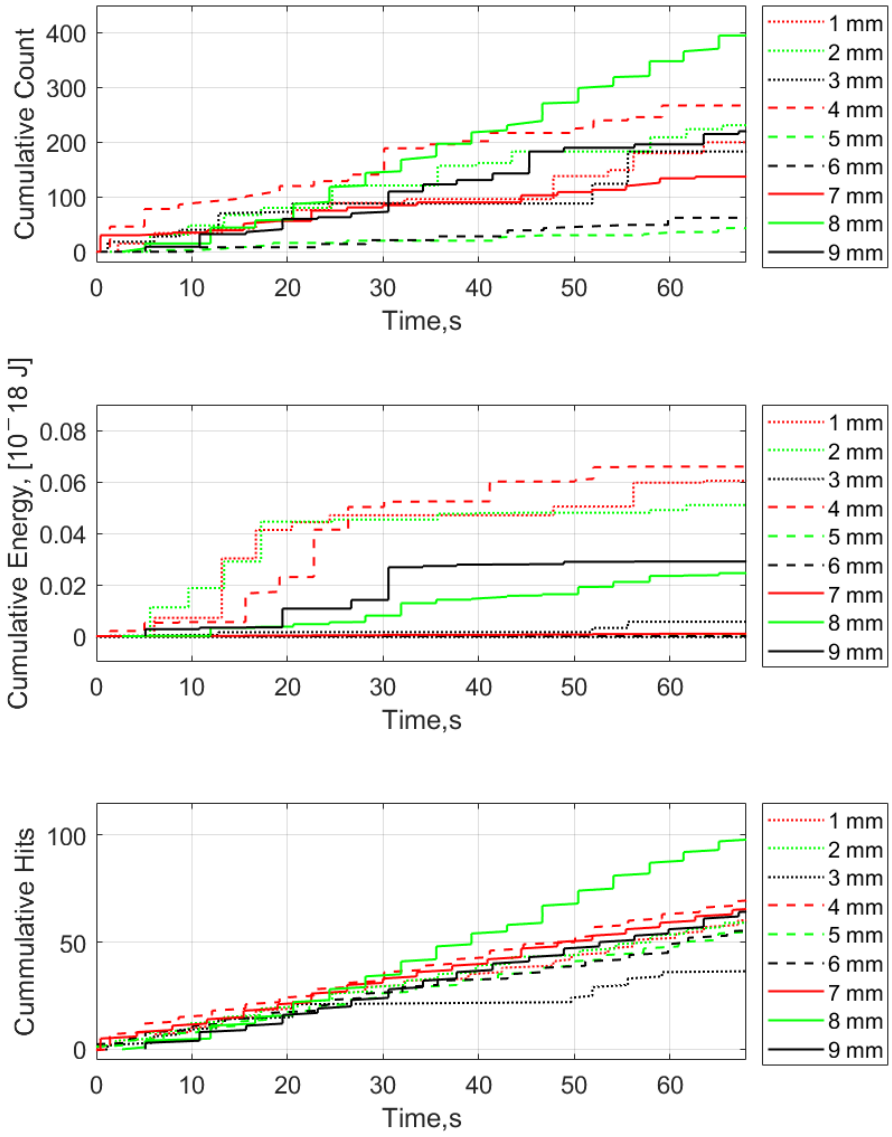

Figure 41: Cumulative AE Count, Energy and Hits trends during one minute leaks monitoring per nozzle.

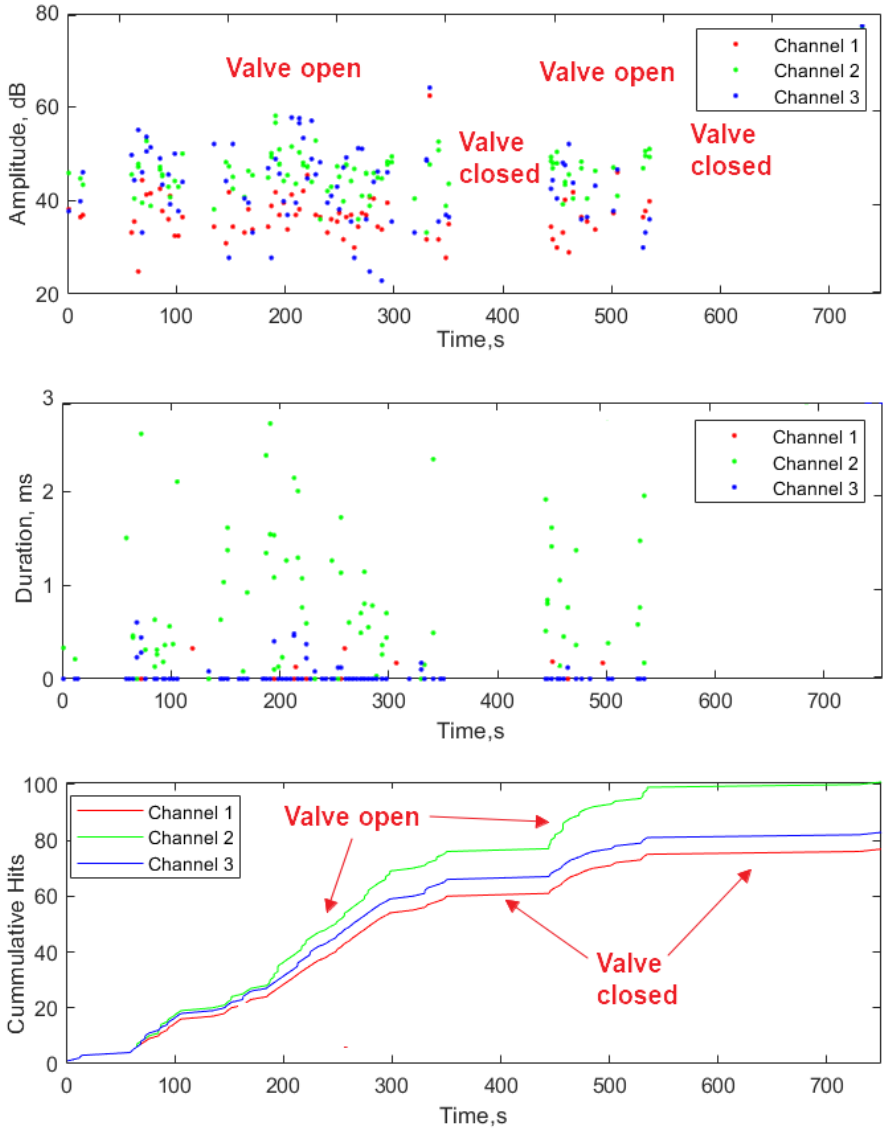

Figure 42: Amplitude, duration and cumulative hits for the AE recorded at Channel 1 to 3 for the 1 mm nozzle.

work of Bogomolov et al. (2021a).

750 seconds monitoring.

A longer monitoring phase, of duration equal to 750 seconds, was performed. Figure 42 shows the AE events in terms of Amplitude in dB and Duration in ms, and the Cumulative Hits for the 1 mm nozzle. As it can be seen, closed and open valve conditions are clearly visible.

The results confirm the possibility of detecting and monitoring leaks of various diameters in the low-frequency region ($1-2$ kHz) not traditionally considered by state-of-art acoustic-emission monitoring systems.

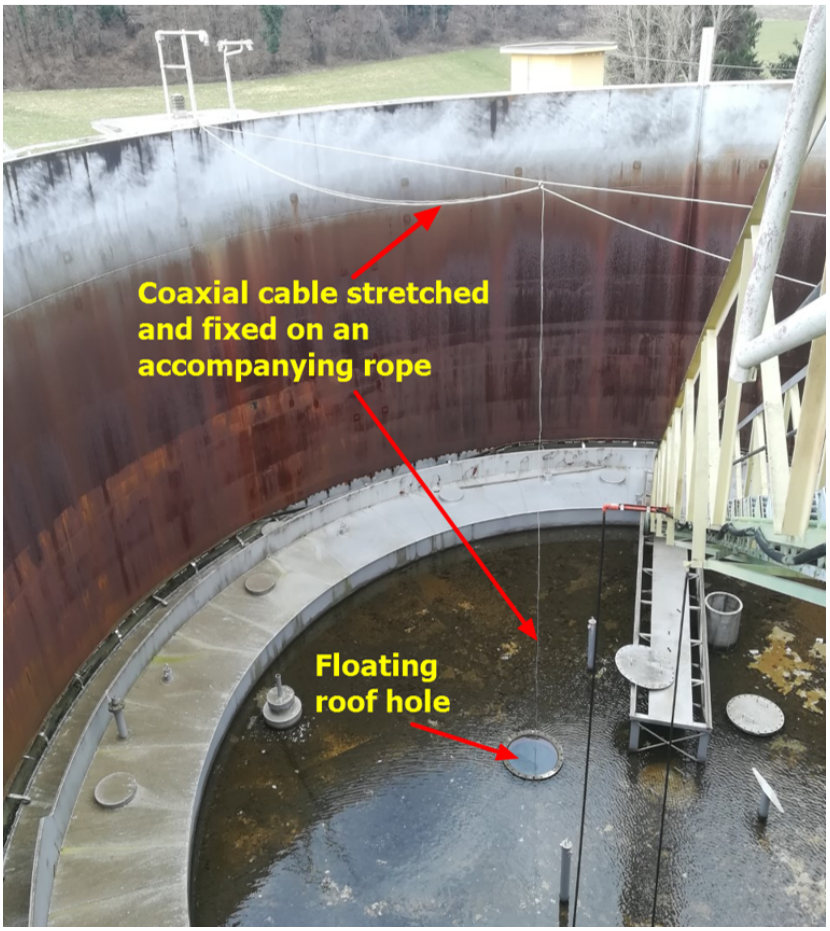

Figure 43: Photo of the experimental setup.

5.2.2 Location algorithm test

To stimulate the AE from the bottom floor of the tank, imitating corrosion activity, a piezo buzzer was immersed in the tank close to the bottom and used as an actuator of acoustic bulk waves in the fluid. As for safety reasons the access to the floating roof of tank was restricted, the actuator and the electrical cable were lowered to the tank floor trough a system of ropes as it can be seen from Figure 43. The chain of measuring and auxiliary equipment assembled to excite the piezo buzzer and to record the AE events from the outer side of the tank was used the same as for the small-scaled storage tank (see Figure 44).

At first, an AE-like signal was mathematically modelled in MATLAB combining a sigmoid and an exponential function, then loaded into the memory of the arbitrary waveform generator (AWG) Agilent 33220A, and used as a signal/waveform to be sent to the amplifier. The waveform was stretched in order to generate AEs with a central frequency content from 50 kHz to 350 kHz using a step of 10 kHz. For each frequency, the voltage provided by the amplifier and read by the oscilloscope (Textronix DPO3014) was adjusted to be 200 V peak to

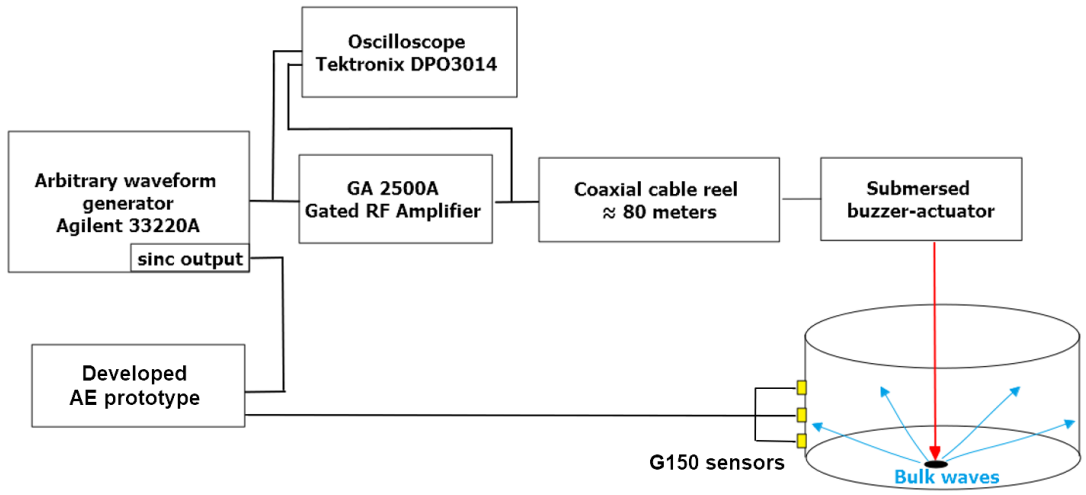

Figure 44: The schematic connection of the equipment for location algorithm test.

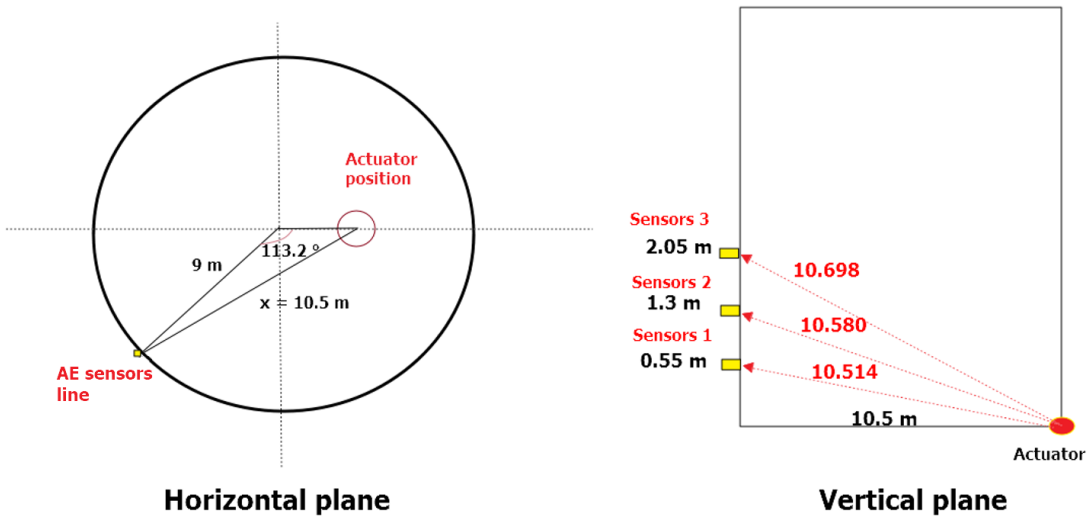

Figure 45: Estimated distance between the actuation source and the sensors lines.

peak.

The target position of the actuator on the tank floor was estimated indirectly as schematically shown in Figure 45 and the wave speed in the water was assumed equal to 1522 m/s. Since only one sample sensor node consisting of three AE channels was manufactured at the time of the experiment, only the innovative algorithm for positioning based on a vertical line of three sensors was tested, bypassing the subsequent multilateration problem considered to have been solved in the literature.

Similar to the small-scaled storage tank experiment, the obtained dToA based on ToAs estimated by Akaike Information Criterion were used to feed the location algorithm. For example, the positions of the three sensors, the level of the water level, the distance between the AE source and the vertical line of the sensors

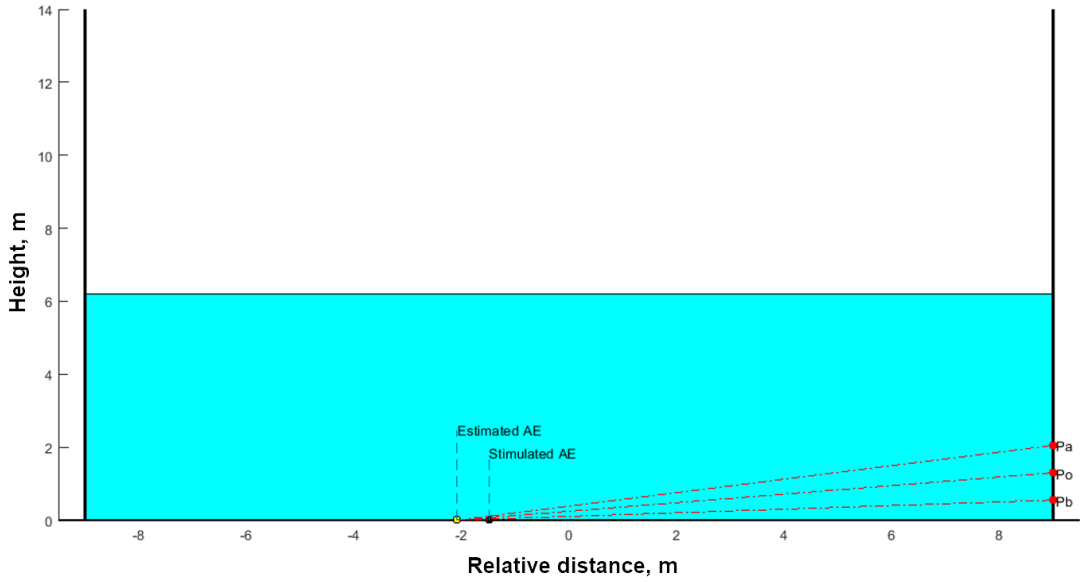

Figure 46: 100 kHz-AE Source location by the three 150 kHz AE sensors line.

Table 7: Error estimation of the location algorithm

Excitation frequency, kHz	Absolute error, m (and relative error, %)
50	1.52 (8.47)
100	0.83 (4.61)
150	0.59 (3.32)
200	0.68 (3.78)
250	0.08 (0.46)
300	0.59 (3.3)
350	0.91 (5.05)

(estimated geometrically as per Figure 46) as well as the distance source-vertical line of the sensors computed by the location algorithm, are shown in Figure . The plot refer to waveforms obtained for the excitation signal centred at 100 kHz. Analogues results for the other input frequencies, from 50 kHz to 350 kHz at a step of 50 kHz, are provided in the Appendix B.

The absolute and relative errors on the AE source location out of these analyses are collected in Table 7. The relative error is computed considering the tank diameter (18 m).

Table 2 shows that the location algorithm combined with a 150 kHz array of probes provides very accurate localization results at the 10 percent level over the entire test frequency range of 50-350 kHz.

6 Discussion Chapter

This section reveals the key findings obtained during the research and development of the AE prototype. Then the connection between the theoretical framework and the results obtained is discussed. Since the work targets posed relate to overcoming both technological (development of a low–cost AE prototype) and modeling (AE location model of AST bottom corrosion) challenges, these aspects will be discussed in different subsections.

6.1 Acoustic Emission Sensor Node

In this work, an innovative, miniaturized low–cost acquisition system able to acquire, pre–process and characterize AE signals for real-time and long-term has been proposed. A detailed mechanism of AE signal processing and extraction of AE parameters from a raw signal such as Peak Amplitude, Rise Time, Duration, Energy and AE Counts, as well as its implementation on STMicroelecronics STM32F3 microcontroller are presented. For preliminary validation of the correctness of the calculation of integrated parameters, a metrological scheme of AE simulation is presented. Then the developed system was successfully verified in the mode of relatively long monitoring, demonstrating changes in AE trends when the signal is excited by a PZT diaphragm placed on a 1000 mm x 1000 mm square plate. As has been demonstrated, the developed AE system can be equipped with two types of sensors: i) a low-cost and low frequency PZT disk with a developed pre–amplifier which was embedded and packed in the same protective case, and ii) high frequency passive G150 AE sensors. One of the key features of the developed prototype of the AE system is its low–cost, estimating the prime cost of the kit of the AE system proposed in this work at less than $ 250 that is partly achieved due to the use of inexpensive piezoelectric buzzer discs as the basis for the AE transducer equipped with a signal pre–amplifier.

The focus of testing of the developed prototype was then shifted on a specifically built small–scaled water storage tank. The high sensitivity of the developed system sensors deployed on the tank wall to bulk waves travelling out through the water was confirmed by comparison with the AE commercial Vallen system. The latter system, according to the literature, is used for AE bottom inspection of the AST, therefore it serves as a reliable reference in this context. It is worth noting that the first versions of the developed prototype did not allow to achieve high sensitivity and several cycles of the external signal pre–amplifier upgrade were performed to achieve a high signal–to–noise ratio over a wide frequency range typical for AE inspection of AST.

6.2 Leaks detection

The results showed the successful application of the developed system for leak detection even at a sensor line distance of 23 meters from the leakage source. It is worth paying special attention to the fact that the system uses transducers based on low-cost piezoelectric buzzer disks, confirming the promise of this technology in terms of widespread use due to its price. The results also confirmed the possibility of detecting and monitoring leaks starting from 1 mm in diameter in the low-frequency region (1-2 kHz) which not traditionally considered by state-of-art acoustic-emission monitoring systems. However, the ability to classify between different leaks requires longer data recording and additional data analysis.

6.3 Alternative AE source location model for AST bottom

The proposed model for locating the AE source on the bottom of the tank was preliminary tested on the small–scaled storage tank. The solution of the proposed problem of three-dimensional location consisted in solving three technical complex sub–problems: i) high-precision detection of the ToAs, ii) development of a mathematical model of the location of the source based on one vertical line of three sensors (alternatively, a model in the form of a star of four sensors is also presented) and iii) solution of the problem multilateration combining coordinates from several vertical lines of sensors (obtained in step ii) whose mathematical model has already been described in detail in the literature.

To solve sub–problem i) the dataset simulated in COMSOL was used, as well as a set of signals recorded on a small tank. It was found that the classical approach in AE in detecting of the signal ToA when the threshold amplitude value is crossed is not applicable when the distance between the sensors is not relatively large. High efficiency has been demonstrated using Akaike Information Criterion, even in comparison with other powerful methods such as cross-correlation of signals (see Figure 23). Then an innovative mathematical model based on the location of the AE source using a vertical line of three sensors is disclosed in 4.2.3 as the solution of ii), while multilateration sub–problem iii) mathematically described in 4.2.4. The experiment on simulating condensate drops also proved the ability to detect the direction of waves propagation from the top based on the DToAs even in relatively short distances between sensors (0,4 m), and as a result to filter out false alarms of the system.

When verifying the three-step algorithm on the small tank, the average location error was equal to 14 cm. As it was investigated by raw signals study, the location accuracy of the proposed algorithm could be limited by the following reasons:

- due to the small size of the tank the waves are reflected from the water table and the tank walls several times, creating interference waves that are not seen in on-field tanks where the tank dimension and the level of the stored liquid are significantly higher;
- the presence of guided ultrasonic waves excited by the immersed piezo and traveling along the tank walls which compromise the received signals by overlapping to the expected bulk waves; these guided waves are not expected in real tanks due to both the complexity of the bottom floor of the tanks (welded and overlapped plates) as well as due to the larger distances and leakage of the waves in the ground;
- the short distance adopted (0.4 m) between the AE sensors deployed in a line reduces the resolution in the target location.

Given the above, this experiment required additional investigation on a full-scale storage tank. Since only one sample of the AE sensor node consisting of three AE channels was manufactured at the time of the experiment on the real storage tank, only the innovative algorithm for positioning based on a vertical line of three sensors was tested, bypassing the subsequent multilateration problem considered to have been solved in the literature.

Summarizing the results of the experiment, location errors were observed depending on the central frequency of the excited signal. Nevertheless, the maximum error at frequency of 50 kHz did not exceed 8,5 %, while the average error among all seven experiments was equal to 4 %, which corresponds to the acceptable limits according to the technical specifications set out in 1. Observation of a cleaner signal when the signal was excited from inside a large tank confirmed the hypotheses outlined above related to the influence of re-reflected waves and minimal attenuation in the small tank.

7 Conclusions

In this work, the Ph.D candidate presented a miniaturized acquisition system able to acquire, pre–process and characterize AE signals for real-time and over time for SHM applications. One of the key features of the developed prototype of the AE system is its low–cost. To be more illustrative, the cost of a leak monitoring kit consisting of three Murata-based sensors presented, one AE sensor node, a gateway and cables is estimated at less than $250. This is partly achieved due to the use of inexpensive piezoelectric buzzer discs as the basis for the AE transducer equipped with a signal preamplifier. Moreover, the proposed sensor–near monitoring paradigm, i.e. the capability to process signals in close proximity to AE transducers at the inspected facility, permits a consistent reduction in the length of the coaxial cables traditionally used by AE bulk instrumentation. Hence this immediate byproduct minimizes the sensitivity to external noise which is the general key reason for the poor SNR of AE equipment *in situ*. Given the fact that the ability to detect changes in AE trends due to structural degradation is a key aspect of long-term monitoring, the developed AE prototype was successfully tested in laboratory.

As another innovative aspect, an alternative configuration of AE sensors and corresponding mathematical model of bottom corrosion localization in AST, is proposed and verified by *in situ* experimental campaign. Particular attention is paid to the experimental setup, because there are few references in the literature to controlled methods of simulating the AE source. For instance, a relatively easy–to–follow scheme for controlled calibration of location algorithms by placing an electrically isolated PZT disk inside a tank at a position with known coordinates is proposed. Tests organized on a real Above Ground Storage tank demonstrated the high accuracy of the proposed algorithm with a relative error of no more than 8.5 % when emitting a signal with a maximum energy at a frequency of 50 kHz, and a minimum error of 0.5 % of a 250 kHz signal.

Finally, the developed system was tested to detect leaks from 1 to 9 mm in the same AST. The results showed the successful application of the developed system. It is worth paying special attention to the fact that the system uses transducers based on low-cost piezoelectric buzzer disks, confirming the promise of this technology in terms of widespread use due to its price. The results also confirmed the possibility of detecting and monitoring leaks of various diameters in the low-frequency region ($1 - 2\,\text{kHz}$) not traditionally considered by state-of-art acoustic-emission monitoring systems.

A Appendix

Decision tree of the AE feature extraction algorithm

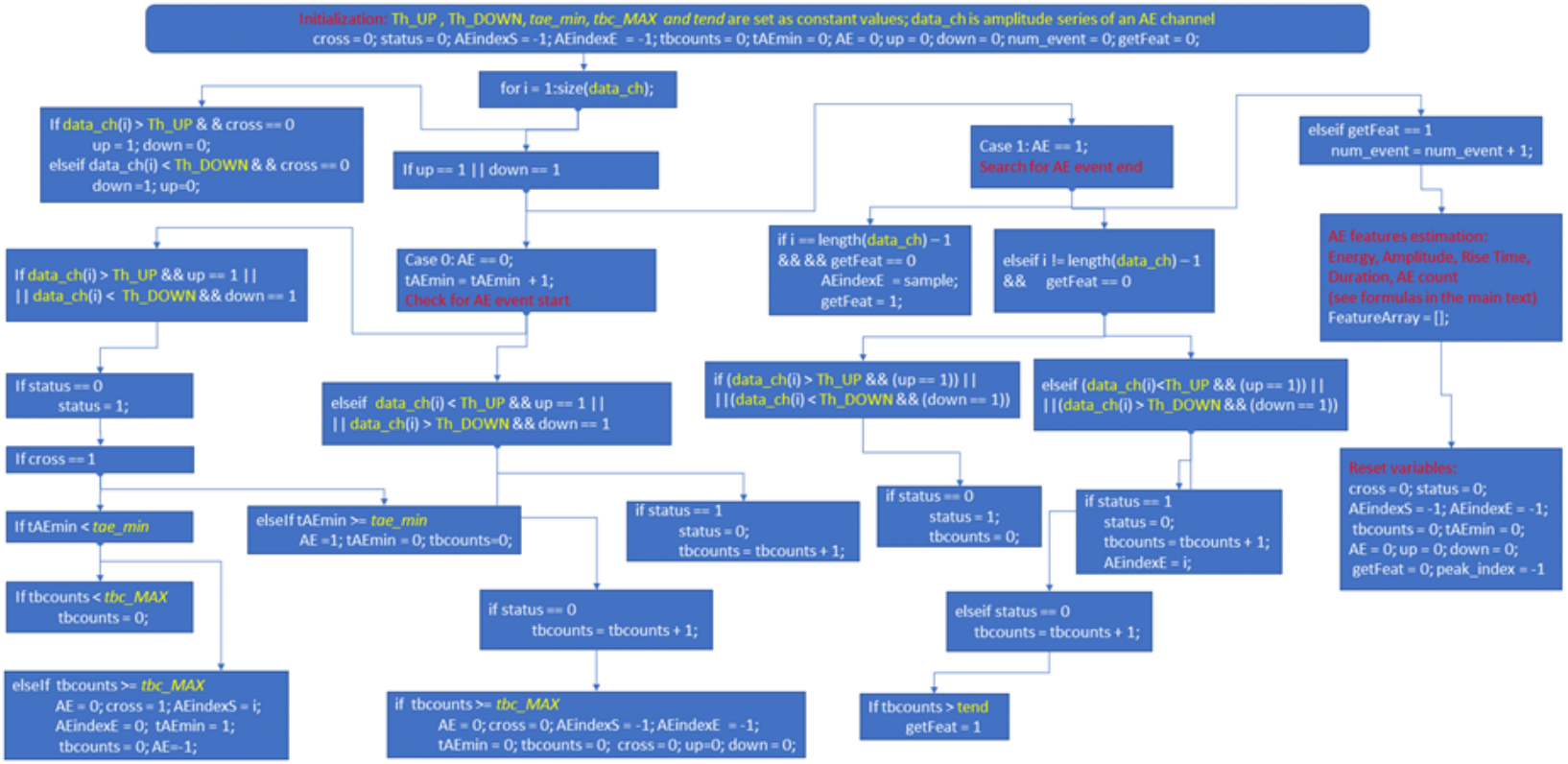

If the «if» condition has no alternative solution in the decision tree (logical state «else»), the second logical state implies "end" and transition to the next sample «i» of the data_ch (next sample of «for» loop).

B Appendix

50 kHz-AE Source localization by the three 150 kHz AE sensors line:

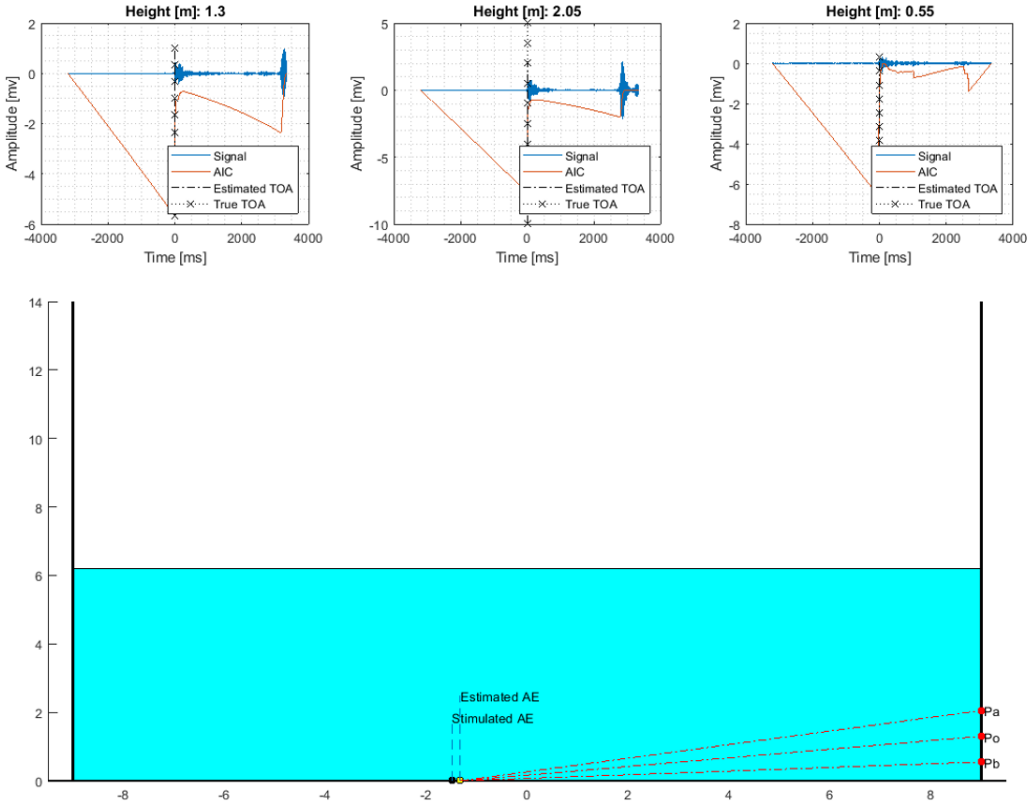

100 kHz-AE Source localization by the three 150 kHz AE sensors line:

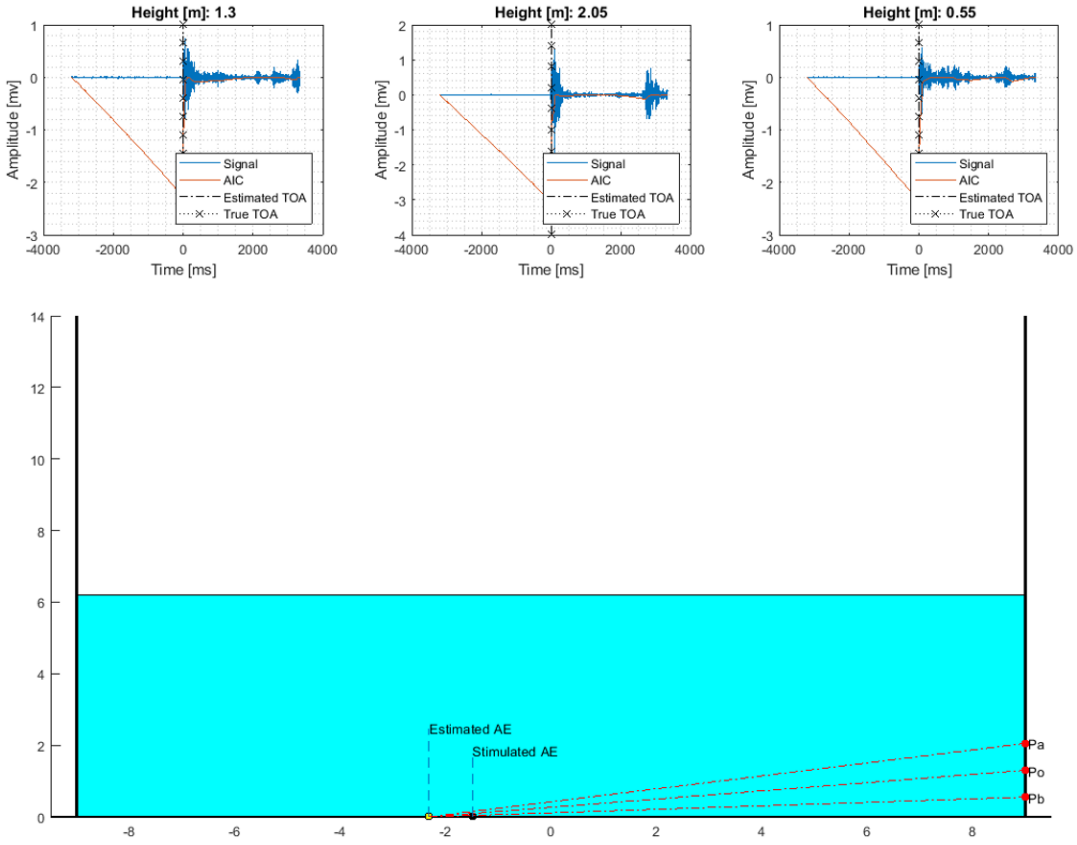

150 kHz-AE Source localization by the three 150 kHz AE sensors line:

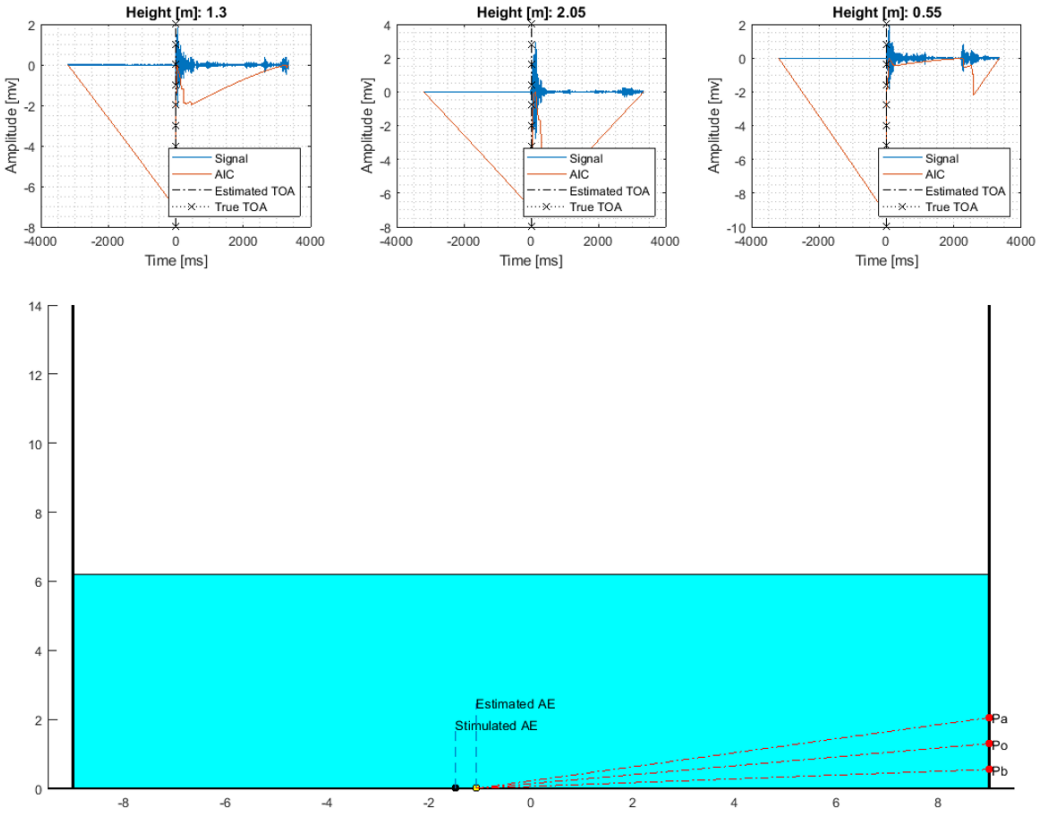

200 kHz-AE Source localization by the three 150 kHz AE sensors line:

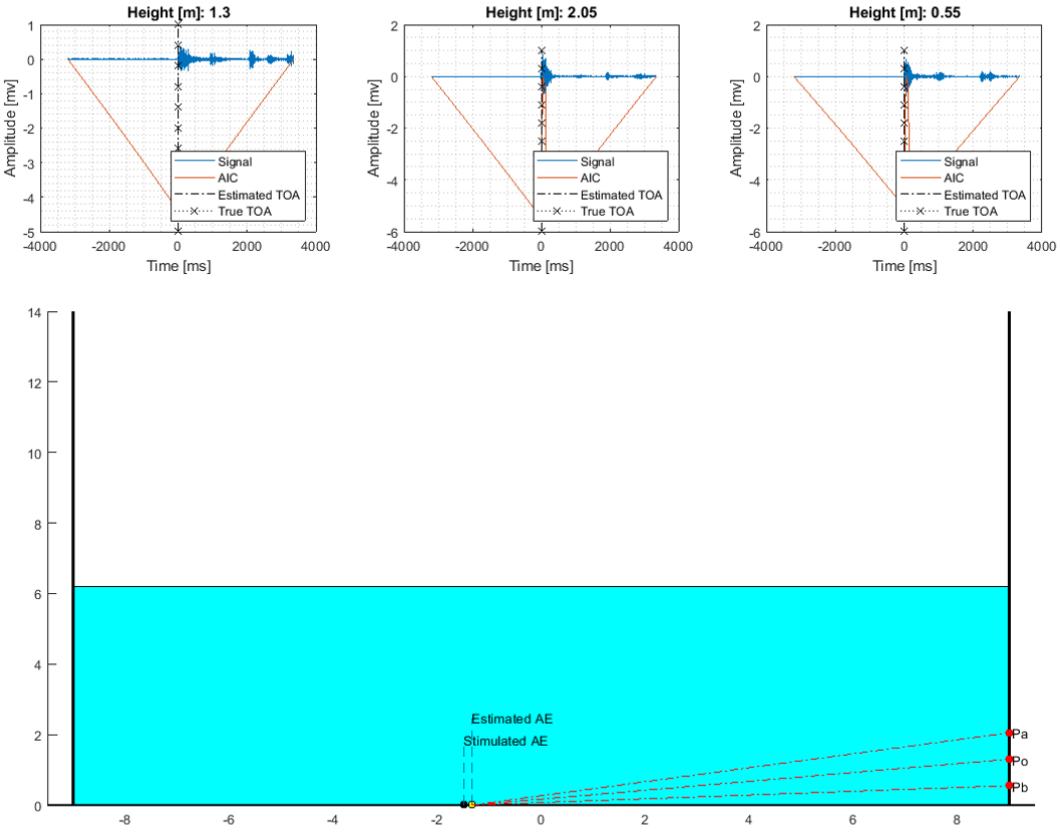

250 kHz-AE Source localization by the three 150 kHz AE sensors line:

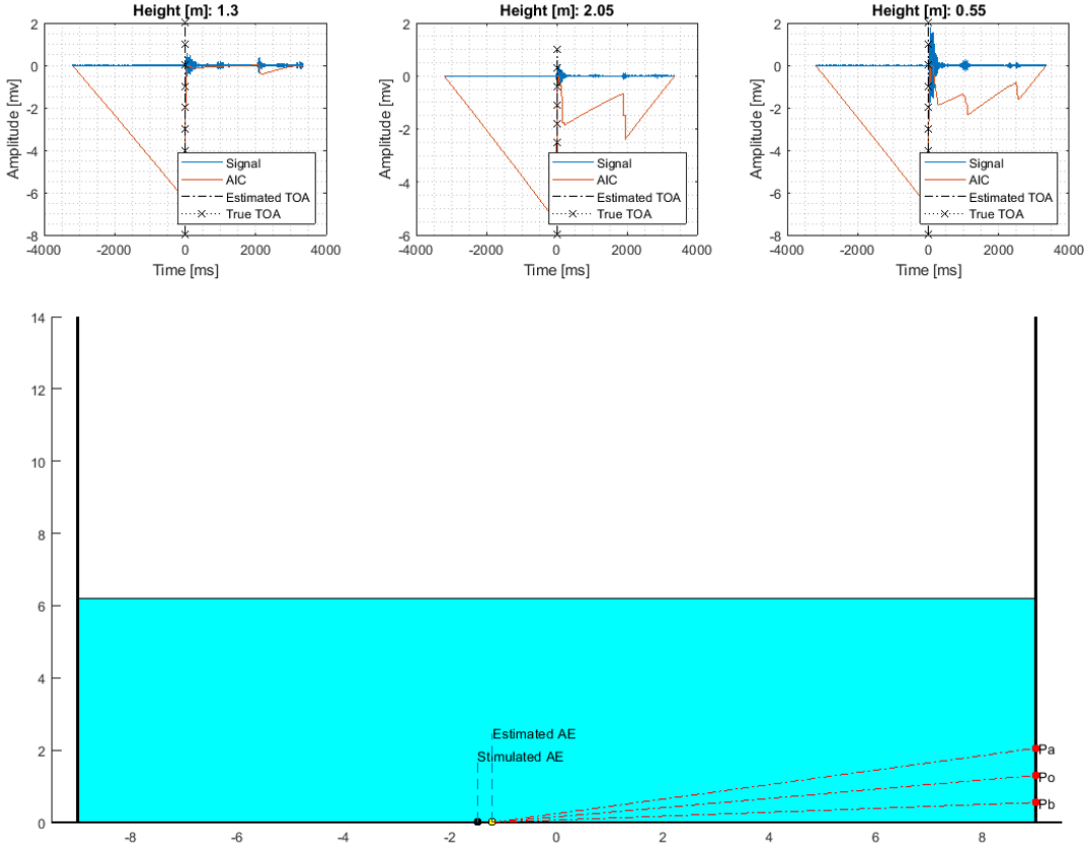

300 kHz-AE Source localization by the three 150 kHz AE sensors line:

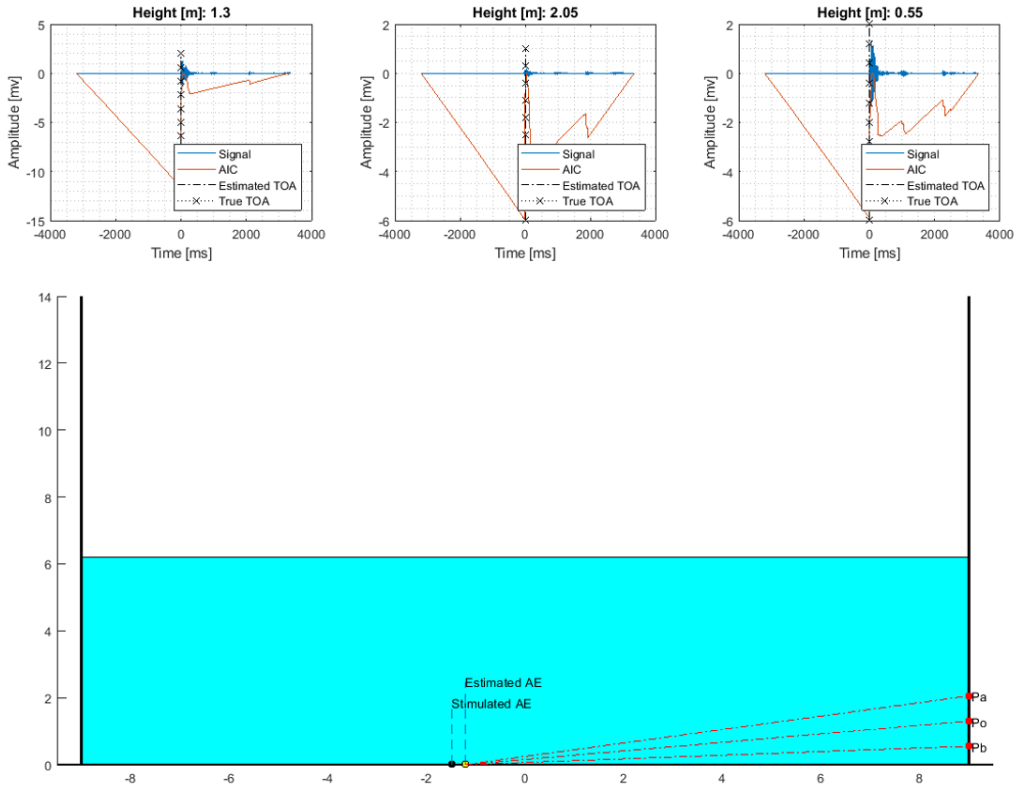

350 kHz-AE Source localization by the three 150 kHz AE sensors line:

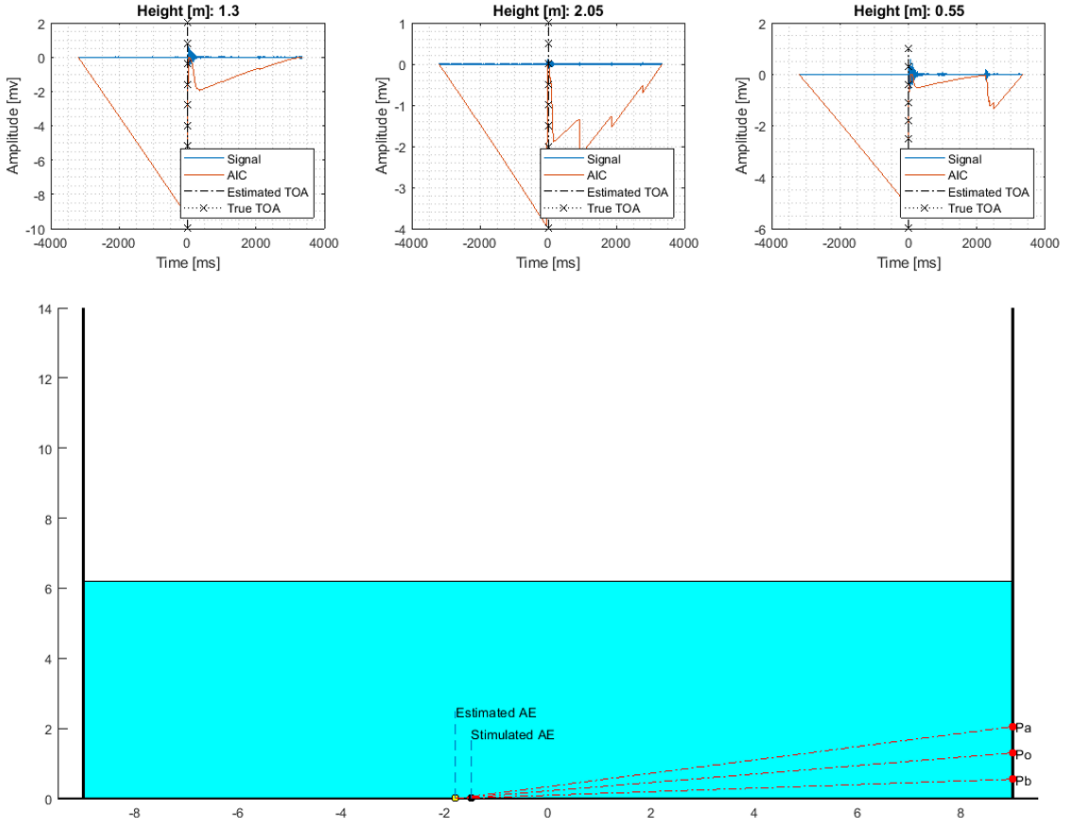

References

ASTM E1930 / E1930M - 17. Standard Practice for Examination of Liquid-Filled Atmospheric and Low-Pressure Metal Storage Tanks Using Acoustic Emission.

ISO/CD 24489. Non-destructive testing — Acoustic emission testing. Corrosion of atmospheric pressure metallic storage tank floor.

API RP 652, Linings of Aboveground Petroleum Storage Tank Bottoms, 3rd ed., 2005.

CBS EN 15856:2010, Non-destructive testing — Acoustic emission. General principles of AE testing for the detection of corrosion within metallic surrounding filled with liquid., 2010.

A. Aljarah, N. Vahdati, and H. Butt. Magnetic Internal Corrosion Detection Sensor for Exposed Oil Storage Tanks. *MDPI, Sensors*, 21(7: 2457), 2021. 10.3390/s21072457.

D. Allsopp, K. J. Seal, and C. C. Gaylarde. *Introduction to biodeterioration.* Cambridge University Press, 2004.

J. Been. Comparison of the corrosivity of dilbit and conventional crude, 2011.

A. Belisario-Briceño, S. Zedek, T. Camps, R. François, C. Escriba, and J. Fourniols. Shm based on modal analysis: accelerometer and piezoelectric transducers instrumentation for civil engineering in heterogeneous structures. In *EWSHM-7th European Workshop on Structural Health Monitoring*, 2014.

D. Bogomolov, N. Testoni, L. de Marchi, T. Borzone, A. Terribile, G. Giunta, and A. Marzani. Aboveground Storage Tanks Leak Detection Through Acoustic Emission Sensor Nodes. volume 2021 48th Annual Review of Progress in Quantitative Nondestructive Evaluation of *Quantitative Nondestructive Evaluation*, 2021a. 10.1115/QNDE2021-75182. URL `https://doi.org/10.1115/QNDE2021-75182`. V001T11A011.

D. Bogomolov, N. Testoni, F. Zonzini, M. Malatesta, L. de Marchi, and A. Marzani. Acoustic emission structural monitoring through low-cost sensor nodes. In *10th International Conference on Structural Health Monitoring of Intelligent Infrastructure*, 2021b.

R. Carlos, M.F.and Miller and T. Tamutus. Acoustic emission local area monitoring system. In *Structural Materials Technology IV - An NDT Conference*, pages 173–178, 2000.

A. Carpinteri, J. Xu, G. Lacidogna, and A. Manuello. pages 529–537, title = Reliable onset time determination and source location of acoustic emissions in concrete structures, journal = Cement and Concrete Composites, 2012.

H. Cho, G. Watanabe, A. Yonezu, H. Suzuki, and M. Takemoto. Corrosion monitoring of tank floor plates by acoustic emission. *Zairyo-to-Kankyo*, 55(9): 406–412, 2006. 10.3323/jcorr.55.406.

S. Elizarov, V. Barat, D. Terentyev, P. Kostenko, V. Bardakov, A. Alyakritsky, V. Koltsov, and P. Trofimov. Acoustic emission monitoring of industrial facilities under static and cyclic loading. *Applied Sciences*, 8:1228, 2018.

R. Ferrari, F. Pioldi, E. Rizzi, C. Gentile, E. Chatzi, E. Serantoni, and A. Wieser. Fusion of wireless and non-contact technologies for the dynamic testing of a historic rc bridge. *Measurement Science and Technology*, 27, 2016. 10.1088/0957-0233/27/12/12401.

Z. A. Foroulis. Magnetic internal corrosion detection sensor for exposed oil storage tanks. *Anti-Corrosion Methods and Materials*, 28(9):4–9, 1981.

S. Generis. Avoid expensive storage tank leaks and spills before they happen!, 2019. URL `https://www.suigeneris.co.uk/blog/avoid-storage-tank-leaks-and-spills`.

C. Grosse, G. McLaskey, S. Bachmaier, S. Glaser, and M. Krüger. A hybrid wireless sensor network for acoustic emission testing in shm. In *Sensors and Smart Structures Technologies for Civil, Mechanical, and Aerospace Systems, 2008*, volume 6932, 2008. https://doi.org/10.1117/12.775641.

A. Groysman. Corrosion of aboveground fuel storage tanks. *Materials performance*, 44(9):44–48, 2005.

A. Groysman. *Corrosion for Everybody*. Springer, Israel, 2010.

N. Groysman, A.and Erdman. A study of corrosion of mild steel in mixtures of petroleum distillates and electrolytes. *CORROSION*, 56 (12):1266–1271, 2000. 10.5006/1.3280515.

E. Hodaei, M. Javadi, A. Broumandnia, and H. Sadeghi. Evaluation of acoustic emission inspection of oil tank floor via tank bottom plates thickness measurement. *Mechanical Research and Application*, 4:37–44, 2012.

InspectAPedia. Oil tank leaks or oil tank tank piping failure oil leak odor causes. URL `https://inspectapedia.com/oiltanks/Oil_Tank_Leak_Causes.php`.

M. Johnson, D. Ozevin, G. Washer, K. Ono, R. Gostautas, and T. Tamutus. Acoustic emission method for real-time detection of steel fatigue crack in eye-bar. *Transportation Research Record: Journal of the Transportation Research Board*, 2313:72–79, 12 2012. 10.3141/2313-08.

J. Kober, Z. Prevorovsky, and M. Chlada. In situ calibration of acoustic emission transducers by time reversal method. *Sensors and Actuators A Physical*, 240: 50–56, 2016. 10.1016/j.sna.2016.01.033.

D. I. G. Krampikowska A, Pała R. The use of the acoustic emission method to identify crack growth in 40crmo steel. *Materials (Basel)*, 12,13 2140, 06 2019. 10.3390/ma12132140.

J. Kurz, C. Grosse, and H.-W. R. Strategies for reliable automatic onset time picking of acoustic emissions and of ultrasound signals in concrete. *Ultrasonics*, 43:538–546, 06 2005.

G. Lackner and P. Tscheliesnig. Acoustic emission testing on flat-bottomed storage tanks: how to condense acquired data to a reliable statement regarding floor condition. *Journal of Acoustic Emission*, 20:179–187, 2003a.

G. Lackner and P. Tscheliesnig. Field testing of flat bottomed storage tanks with acoustic emission - a review on the gained experience. 2003b.

G. Lackner and P. Tscheliesnig. Acoustic emission (ae) field application: Testing of aboveground storage tanks (ast) for corrosion and leakage. In *Researchgate*, pages 8–12, 2007.

A. Ledeczi, T. Hay, P. Volgyesi, D. Hay, A. Nadas, and S. Jayaraman. Wireless acoustic emission sensor network for structural monitoring. *IEEE Sensors Journal*, 9:1370–1377, 2009. doi:10.1109/JSEN.2009.2019315.

X. Li, X. Shang, A. Morales-Esteban, and Z. Wang. Identifying p phase arrival of weak events: The akaike information criterion picking application based on the empirical mode decomposition. *Computers & Geosciences*, 100:57–66, 2017.

M. Malatesta, F. Zonzini, D. Bogomolov, N. Testoni, L. De Marchi, and A. Marzani. Structural health monitoring reliability enhancement by an automated sensor tuning procedure. 2020.

G. Martin. Acoustic emission for tank bottom monitoring. In *Key Engineering Materials, 4th Asia Pacific Workshop on Structural Health Monitoring At: Melbourne, Australia*, 2012. 10.4028/www.scientific.net/KEM.558.445.

S. Martinez. Estimating internal corrosion rate and internal inspection interval of aboveground hydrocarbon storage tanks. *Goriva i Maziva/Fuels and Lubricants*, 52(2):134–143, 2013.

H. Mazille, R. Rothea, and C. Tronel. An acoustic emission technique for monitoring pitting corrosion of austenitic stainless steels. *Corrosion Science*, 37(9):1365–1375, 1995. ISSN 0010-938X. https://doi.org/10.1016/0010-938X(95)00036-J. URL `https://www.sciencedirect.com/science/article/pii/0010938X9500036J`.

L. Mažeika, R. Kažys, R. Raišutis, A. Demčenko, and R. Šliteris. Long-range ultrasonic non-destructive testing of fuel tanks, 2006.

Y. Mori, M. Shiwa, M. Nakano, and K. Iwai. New concept of ae standard : Jis z 2342-2002 " method for acoustic emission testing of pressure vessels during pressure tests and classification of test results ". 2004.

K. Morofuji, N. Tsui, M. Yamada, A. Maie, S. Yuyama, and Z. W. Li. Quantitative study of acoustic emission due to leaks from water tanks. In *Journal of Acoustic Emission*, volume 21, page 213, 2003.

A. Norrdine. An algebraic solution to the multilateration problem. 04 2015. 10.13140/RG.2.1.1681.3602.

M. R. Pearson, M. Eaton, C. Featherston, R. Pullin, and K. Holford. Improved acoustic emission source location during fatigue and impact events in metallic and composite structures. *Structural Health Monitoring*, 16(4):382–399, 2017.

A. A. Pollock. *Acoustic Emission Inspection, Metals handbook.* ASM international, 1989.

A. Prateepasen. *Pitting Corrosion Monitoring Using Acoustic Emission.* 01 2012. ISBN 978-953-51-0275-5. 10.5772/33127.

R. Pullin, M. Eaton, J. Hensman, K. Holford, K. Worden, and S. Evans. Validation of Acoustic Emission (AE) Crack Detection in Aerospace Grade Steel Using Digital Image Correlation. *Applied Mechanics and Materials*, 24-25:221–226, 06 2010. 10.4028/www.scientific.net/AMM.24-25.221.

M. Riahi and H. Shamekh. Health monitoring of aboveground storage tanks' floors: A new methodology based on practical experience. *Russian Journal of Nondestructive Testing*, 42(8):537–543, 2006.

F. G. Rivera, G. Edwards, E. Eren, and S. Soua. Acoustic emission technique to monitor crack growth in a mooring chain. *Applied Acoustics*, 139:156 – 164, 2018. ISSN 0003-682X. https://doi.org/10.1016/j.apacoust.2018.04.034. URL `http://www.sciencedirect.com/science/article/pii/S0003682X17308289`.

A. Sagaidak, V. Bardakov, S. Elizarov, and D. Terentyev. The use of acoustic emission method in the modern construction. In *Proceedings of the 31st Conference of the European Working Group on Acoustic Emission, Dresden, Germany*, volume 31, 2014.

J. G. Speight. *Overview of corrosion engineering, science and technology,*. Oil and Gas Corrosion Prevention, Gulf Professional Publishing, 2014.

A. St-Onge. Akaike information criterion applied to detecting first arrival times on microseismic data. In *SEG Technical Program Expanded Abstracts 2011*, pages 1658–1662. Society of Exploration Geophysicists, 2011.

A. Tadros. Environmental aspects of petroleum storage in above ground tank. e3s web of conferences. *E3S Web of Conferences*, 166:01006, 2020. 10.1051/e3sconf/202016601006.

M. Teodorczyk. Influence of aggregate gradation on the longitudinal wave velocity changes in unloaded concrete. *IOP Conference Series: Materials Science and Engineering*, 245:032084, 10 2017. 10.1088/1757-899X/245/3/032084.

N. Testoni, L. De Marchi, and A. Marzani. A stamp size, 40ma, 5 grams sensor node for impact detection and location. In *European Workshop on SHM*, 2016.

C. Tong and B. Kennett. pages 1986–1909, title = Automatic seismic event recognition and later phase identification for broadband seismograms, journal = Bull Seismol Soc Am, 1996.

M. J. Whelan, M. P. Fuchs, M. V. Gangone, and K. D. Janoyan. Development of a wireless bridge monitoring system for condition assessment using hybrid techniques. In *Sensor Systems and Networks: Phenomena, Technology, and Applications for NDE and Health Monitoring 2007*, volume 6530, 2007. https://doi.org/10.1117/12.715905.

Y. Wu, W. Liu, and K. Li. A novel wireless acoustic emission sensor system for distributed wooden structural health monitoring. *International Journal of Innovative Computing, Information and Control*, 13:1289–1306, 2017.

T. Yan, P. Theobald, and B. Jones. A self-calibrating piezoelectric transducer with integral sensor for in situ energy calibration of acoustic emission. *NDT and E International*, 35(7):459–464, 2002.

N. Yemashova, V. Murygina, D. Zhukov, A. Zakharyantz, M. Gladchenko, V. Appanna, and S. Kalyuzhnyi. Biodeterioration of crude oil and oil derived products: A review. *Reviews in Environmental Science and Biotechnology*, 6:315–337, 2007. 10.1007/s11157-006-9118-8.

F. Zonzini, D. Bogomolov, T. Dhamija, N. Testoni, L. De Marchi, and A. Marzani. Deep learning approaches for robust time of arrival estimation in acoustic emission monitoring. *IEEE Sensors Journal*, 22, 2022.